

Lithospheric structure in Central Eurasia derived from elevation, geoid anomaly and thermal analysis

ALEXANDRA M. M. ROBERT^{1,2*}, MANEL FERNÀNDEZ¹,
IVONE JIMÉNEZ-MUNT¹ & JAUME VERGÉS¹

¹*Group of Dynamics of the Lithosphere (GDL), Institute of Earth Sciences Jaume Almera, ICTJA-CSIC, Lluís Solé i Sabarís s/n, 08028 Barcelona, Spain*

²*Géosciences Environnement Toulouse, UMR CNRS-IRD-Université de Toulouse, 14 avenue Edouard Belin, 31400 Toulouse, France*

*Correspondence: alexandra.robert@get.obs-mip.fr

Abstract: We present new crustal and lithospheric thickness maps for Central Eurasia from the combination of elevation and geoid anomaly data and thermal analysis. The results are strongly constrained by numerous previous data based on seismological and seismic experiments, tomographic imaging and integrated geophysical studies. Our results indicate that high topography regions are associated with crustal thickening that is at a maximum below the Zagros, Himalaya, Tien Shan and the Tibetan Plateau. The stiffer continental blocks that remain undeformed within the continental collision areas are characterized by a slightly thickened crust and flat topography. Lithospheric thickness and crustal thickness show different patterns that highlight an important strain partitioning within the lithosphere. The Arabia–Eurasia collision zone is characterized by a thick lithosphere underneath the Zagros belt, whereas a thin to non-existent lithospheric mantle is observed beneath the Iranian and Anatolian plateaus. Conversely, the India–Eurasia collision zone is characterized by a very thick lithosphere below its southern part as a consequence of the underplating of the cold and stiff Indian lithosphere. Our new model presents great improvements compared to previous global models available for the region, and allows us to discuss major aspects related to the lithospheric structure and acting geodynamic processes in Central Eurasia.

Supplementary material: Residual geoid anomaly between different order and degree of filtering, our compilation of crustal thickness from publications and our resulting crustal and lithospheric thickness in .txt format are available at: <http://www.geolsoc.org.uk/SUP18846>

The Central Eurasia region contains two of the most prominent deformed regions on Earth: the Arabia–Eurasia and the India–Eurasia collision zones, forming the most part of the well-studied Alpine–Himalayan belt. Defining the lithospheric structure of such a large region, including areas with very scarce information, will provide important contributions to understanding the relevant geodynamic processes occurring in collisional contexts.

During the last decades, the Himalaya–Tibet and Zagros–Iran regions have been the target of numerous geophysical surveys (mostly receiver functions, deep seismic and tomographical studies) to unravel their lithospheric structures. Crustal thickness data include one-dimensional (1D) spotted estimations (e.g. Nasrabadi *et al.* 2008; Chen *et al.* 2010), 2D transects across the Himalaya–Tibet region (e.g. Kind *et al.* 2002; Tian *et al.* 2005; Nabelek *et al.* 2009) or the Zagros–Iran region (e.g. Paul *et al.* 2006, 2010) and 3D regional

studies (e.g. Zor *et al.* 2003; Pan & Niu 2011). However, some other areas of Central Eurasia are less well known owing to the lack of seismological and seismic studies. In fact, less than 19% of the region has crustal-thickness-data coverage better than one measure per 50 000 km² (i.e. one point every 2 × 2 arc-degree). Furthermore, results from these geophysical studies show a high scatter related to different surveys, instrumentation, recording periods and methodology. Some global crustal thickness models are proposed and they have provided general features of the crustal structures with a spatial resolution of up to 1 × 1 arc-degree (e.g. Nataf & Ricard 1996; Mooney *et al.* 1998; Bassin *et al.* 2000; Laske *et al.* 2013). Lithospheric thickness estimations are even scarcer and they are highly variable as a function of the used methodology. Regional tomography models have been developed to image the upper-mantle structure (e.g. Ritzwoller & Levshin 1998; Villaseñor *et al.* 2001) and only a few receiver function studies

have been able to image the base of the lithosphere (e.g. Ramesh *et al.* 2010; Zhao *et al.* 2010).

Jiménez-Munt *et al.* (2012) presented a detailed image of the crust and lithospheric mantle variations in the Arabia–Eurasia collision zone based on the combination of geoid and elevation data, and thermal analysis. In the present study, we use a similar approach with the aim of mapping the crust–mantle boundary (CMB) and the lithosphere–asthenosphere boundary (LAB) over the entire Central Eurasia region that we compare with available data. This study therefore incorporates an up-to-date compilation of crustal thickness data from seismological and seismic studies, including 1212 estimations coming from more than 100 references used as the main constraints. We compare our resulting crustal and lithospheric thickness maps with previous global crustal and lithosphere thermal models (e.g. Artemieva 2006; Goutorbe *et al.* 2011; Laske *et al.* 2013; Reguzzoni *et al.* 2013), and discuss relevant geodynamic processes occurring in the Central Eurasia region.

Geodynamic context

During Cenozoic times, the Central Eurasia region has been affected by the India–Eurasia and Arabia–Eurasia continental collisions. In both cases, collision occurred between the strong and resistant Archean–Proterozoic shields of the Indian and Arabian plates, and the weaker southern margin of Eurasia. The weakness of the Eurasian margin is interpreted to be a result of the presence of major pre-existing structures, such as suture zones, and/or large-scale fault zones between the different accreted Gondwana-derived continental blocks (e.g. Audet & Bürgmann 2011). As a consequence of these collisions, two major topographical features arose: the Zagros and the Himalaya orogenic belts, which show different stages of development owing to differences in the amounts of convergence and the ages of initiation of the collision (Hatzfeld & Molnar 2010).

For the sake of simplicity, we differentiate the region into five major tectonic subdivisions: (1) the Arabian Plate; (2) the Indian Plate; (3) the Arabia–Eurasia collision zone; (4) the India–Eurasia collision zone; and (5) the region to the north of the Tethysides (Fig. 1).

The Arabian Plate

The Arabian Plate is composed of the Arabian shield (Late Proterozoic basement) unconformably overlapped to the east by the Phanerozoic Arabian platform, and separated from Africa by young spreading centres located within the Red Sea and the Gulf of

Aden (Al-Damegh *et al.* 2005). The Arabian platform consists of thick Palaeozoic and Mesozoic sediments dipping to the NE and reaching more than 10 km in thickness (Mokhtar *et al.* 2001). The Red Sea marks the boundary between Africa and Arabia, and consists of both oceanic and thinned continental crust (Al-Damegh *et al.* 2004) covered by up to 5 km-thick Cenozoic sediments, according to the *Exxon Tectonic Map of the World* (Exxon 1994).

The Indian Plate

The Indian Plate is composed of several Early–Late Archean cratons delimited by rift zones containing Proterozoic and/or Phanerozoic sediments (Naqvi & Rogers 1987). The massive basalts of the Deccan volcanic province erupted during the Late Cretaceous–Early Tertiary and are considered to be a consequence of the separation of India from the Seychelles microcontinent (a Gondwana-derived continental block) under the influence of the Réunion mantle plume (Mahoney 1988). The breakup of Gondwanaland occurred around 140 Ma (earliest Cretaceous) and corresponds to the beginning of the northern drift of the Indian Plate towards Eurasia (Kumar *et al.* 2007).

The Arabia–Eurasia collision zone

The Zagros Orogen is the consequence of the closure of the Neotethys Ocean that was located between Arabia and Eurasia (e.g. Sengör *et al.* 1988; Agard *et al.* 2011). Although the timing of the continental collision is still controversial, the final closure of the Neotethys Ocean seems to have occurred during the Late Oligocene–earliest Miocene (e.g. Agard *et al.* 2011; Vergés *et al.* 2011; Mouthereau *et al.* 2012; McQuarrie & van Hinsbergen 2013). The Zagros orogenic system continues to the SE to Makran and its NW continuation corresponds to SE Anatolia, where the collision started earlier than in the Zagros (Agard *et al.* 2011). Subduction-related volcanism continues to occur throughout both the Iranian and the Turkish plateaus (Kazmin *et al.* 1986) suggesting that, despite the change from subduction to continental collision, the tectonics of these plateaus is still driven by subduction processes within the upper mantle (Hearn & Ni 1994; Agard *et al.* 2011). The Alborz and Kopet Dagh ranges developed along the Palaeotethys suture zone (Sengör *et al.* 1988; Robert *et al.* 2014), and they correspond to the northern boundary of the Arabia–Eurasia collision zone. The Alborz is bounded to the north by the South Caspian Sea Basin, which is characterized by a sedimentary basin exceeding 20 km in sediment thickness (Brunet *et al.* 2003) (Fig. 2).

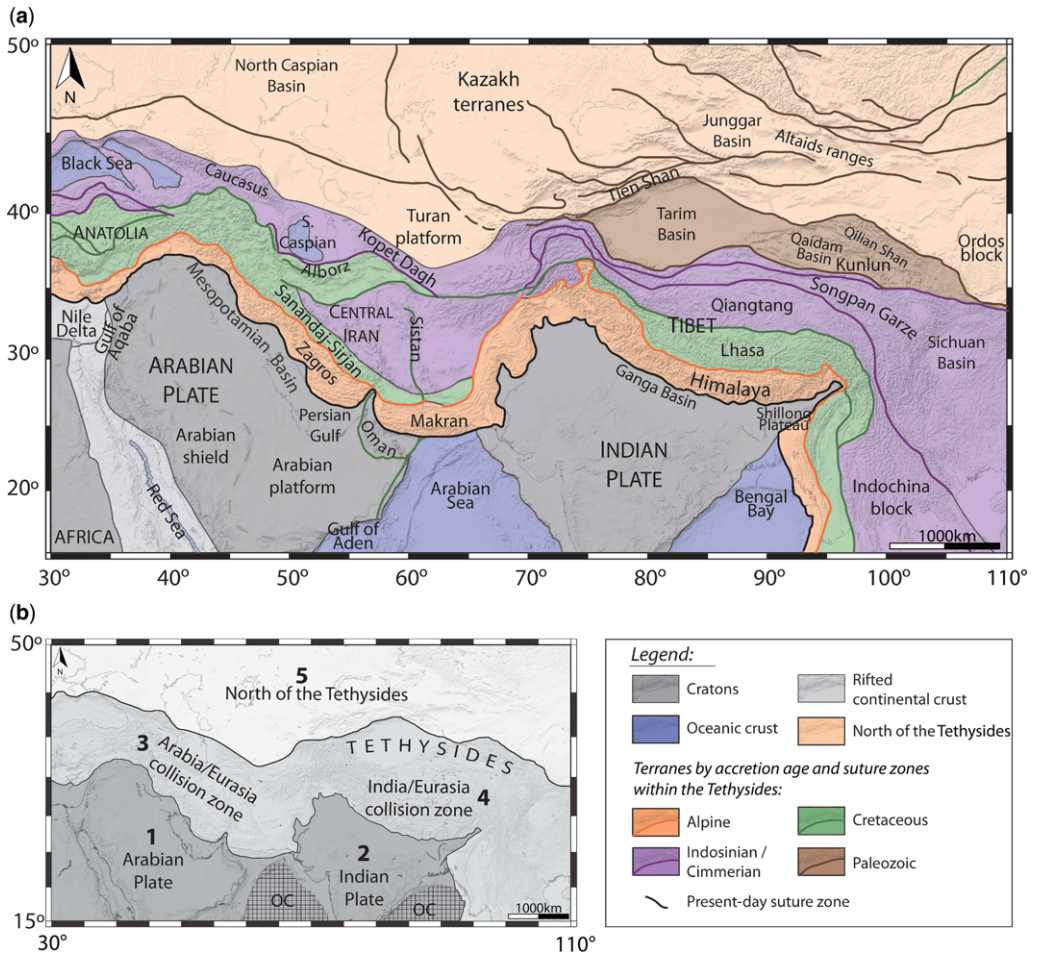


Fig. 1. Simplified structural map of the Central Eurasia region modified from the structural map of Eastern Eurasia (Pubellier *et al.* 2008, modified) and other publications (Sengör & Natal'in 1996; Frizon de Lamotte *et al.* 2013). (a) This map highlights the accreted terranes in the region resulting from the long-lived convergence between Gondwana-derived blocks and the southern margin of Eurasia since the end of the Palaeozoic. (b) Simplified map showing the different zones delimited in this study. OC: Oceanic Crust. The shaded relief was obtained from the ETOPO1 database (Amante & Eakins 2009). The scale bar in kilometres was calculated at 15° of latitude.

The India–Eurasia collision zone

The India–Eurasia collision zone hosts the largest and highest topographical feature on Earth: the Tibetan Plateau, which was built by the sequential accretion of lithospheric terranes on the southern margin of Eurasia since the end of the Palaeozoic (Yin & Harrison 2000; Pubellier *et al.* 2008). From north to south, the Tibetan Plateau is successively formed by: (1) the Kunlun terrane; (2) the Songpan Garze flysch complex related to the closure of the Palaeotethys; (3) the continental Qiangtang terrane accreted at the end of the closure of the Palaeotethys; and (4) the Lhasa terrane

accreted during Cretaceous times (Fig. 1). The Indus Tsangpo suture zone, related to the closure of the Neotethys Ocean, is located to the south of the Lhasa block and to the north of the Himalaya. The timing of the India–Eurasia collision is still subject to controversies but most authors agree that it occurred between 55 and 45 Ma during the Eocene (e.g. Rowley 1996; Zhu *et al.* 2005).

North of the Tethysides

The north of the Tethysides is a region composed from east to west by the Ordos block, the Altaid range (Fig. 1), the Tien Shan range, the Kazakh

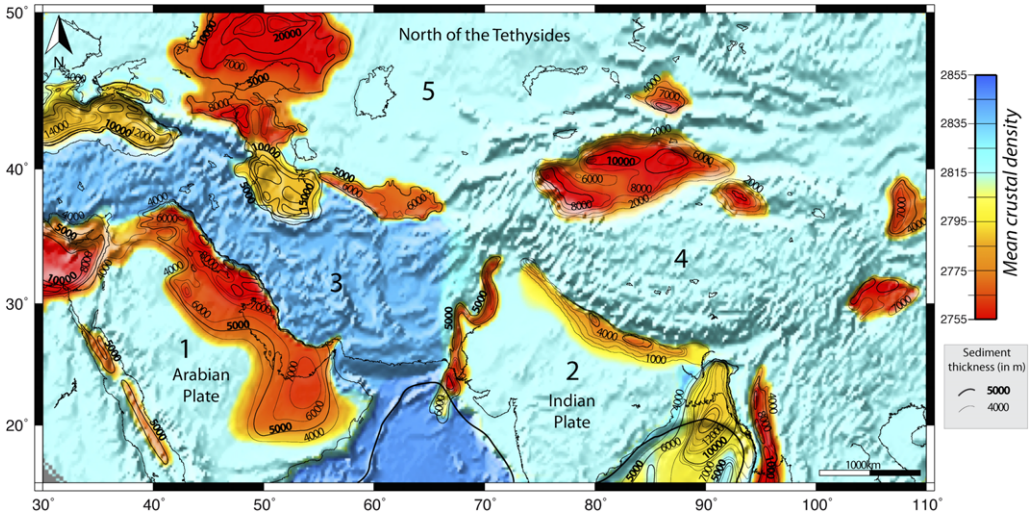


Fig. 2. Mean crustal density used as an input in our model. Contours denote sediment thickness in metres taken from the *Exxon Tectonic Map of the World* (Exxon 1994) and publications referred to in the text. Used parameters for each region are summarized in the Table 2.

terranes, the Turan platform and the North Caspian Basin, the Black Sea and the East European Craton (Fig. 1). The Altai range has a complex geodynamic evolution made of multiple accretions of terranes of different origin, chiefly microcontinents and island arcs occurring from 600 to 250 Ma (latest Precambrian–earliest Triassic times) (Wilhem *et al.* 2012). Numerous sedimentary basins were developed in this area, such as the Junggar Basin or the North Caspian Basin, which present an up to 20 km-thick sedimentary sequence.

Methodology and input data

Method

We calculated the crustal and the lithospheric mantle thickness by combining elevation and geoid data together with thermal analysis in a 1D approach (Fullea *et al.* 2007). This method assumes local isostasy with a depth of compensation below the lithosphere–asthenosphere boundary (LAB) and considers four layers: seawater, crust, lithospheric mantle and asthenosphere. The crustal density increases linearly with depth between predefined values at surface and at the base of the crust. The lithospheric mantle density (ρ_m) is considered to be temperature-dependent:

$$\rho_m(z) = \rho_a(1 + \alpha(T_a - T(z)))$$

where ρ_a is the density of the asthenosphere considered constant everywhere, α is the thermal

expansion coefficient, T_a is the temperature at the LAB and $T(z)$ is the temperature of the lithospheric mantle at a given depth z .

The geoid anomaly is calculated relative to a reference level (H_0), which in turn depends on a selected reference lithospheric column with a known crustal thickness and elevation. It can be demonstrated that knowing the crustal thickness, and considering an average crustal density and heat production, we can calculate the lithospheric thickness that fits the elevation corresponding to the selected reference column (see Fullea *et al.* 2007 for details). The lithospheric reference column for geoid anomaly has been chosen within the Indian shield where consistent crustal and lithospheric thicknesses are obtained from seismic and seismological studies (e.g. Kumar *et al.* 2007; Bhat-tacharya 2009; Ramesh *et al.* 2010). This method was successfully applied to decipher crustal and lithospheric structures in the Gibraltar arc system (Fullea *et al.* 2007) and in the Arabia–Eurasia collision zone (Jiménez-Munt *et al.* 2012).

Input parameters used in our modelling are summarized in Tables 1 and 2. According to the large extent of the region considered, lateral variations of the surface density were used in our modelling (Fig. 2). This 2D density distribution takes into account the occurrence of large sedimentary basins, as well as small differences between the considered tectonic subdivisions (Table 2). Because the crust is defined as a simple layer with a linear depth–density increase, the occurrence of thick sedimentary basins is associated with a decrease in

Table 1. Constant parameters used over the whole Central Eurasia region in our modelling

Parameter	Value
Asthenosphere density (ρ_a)	3200 kg m ⁻³
Seawater density (ρ_w)	1031 kg m ⁻³
Temperature at the LAB (T_a)	1300°C
Surface temperature (T_s)	15°C
Thermal expansion coefficient (α)	$3.5 \times 10^{-5} \text{ K}^{-1}$
Crustal thermal conductivity (k_c)	$2.7 \text{ W K}^{-1} \text{ m}^{-1}$
Mantle thermal conductivity (k_m)	$3.2 \text{ W K}^{-1} \text{ m}^{-1}$

the surface crustal density. First, we obtained the sediment thickness distribution by digitizing the *Exxon Tectonic Map of the World* (Exxon 1994), complemented with some local studies (Sastri *et al.* 1971; Rao 1973; Karunakaran & Rao 1979; Singh 1996) (Fig. 2). Then we calculated the surface density according to:

$$\rho_{\text{surf}} = 2700 - 100 \times \left(1 - \exp\left(-\frac{H}{5}\right) \right)$$

with ρ_{surf} being the crustal density at the surface and H the sediment thickness expressed in km. This relationship has been chosen in order to simulate the lower average crustal density at the surface with the increase in the sediment thickness. According to this equation, the surface density is equal to 2700 kg m⁻³ when there is no sediments and equal to 2602 kg m⁻³ when sediments are 20 km thick.

Certainly, the absolute density values used for the lithospheric mantle and the asthenosphere are noticeably lower than the actual ones. This is because we are using a ‘pure’ thermal approach in which the lithosphere mantle density is only temperature-dependent and the density of the asthenosphere is constant everywhere. In other words, temperature is the dominant effect on density and no pressure effects are considered. Note that this approach is widely used in describing variations of

topography and potential fields since they mainly depend on lateral density variations rather than on absolute density values.

Because of the occurrence of large magmatic provinces and numerous ophiolitic belts, the crustal density at Moho depth in the Arabia–Eurasia collision zone has been increased to 2970 kg m⁻³. We use classical thermal conductivities of $2.7 \text{ W m}^{-1} \text{ K}^{-1}$ for the crust and $3.2 \text{ W m}^{-1} \text{ K}^{-1}$ for the lithospheric mantle. The thermal conductivities are considered as constant in our modelling. In fact, the larger variability of the crustal thermal conductivity is restricted to the uppermost part of the crust (up to 20 MPa) (Clauser & Huenges 1995) and then does not much affect the average crustal thermal conductivity. The average crustal radiogenic heat production is $0.5 \mu\text{W m}^{-3}$ for continental crust and $0.3 \mu\text{W m}^{-3}$ for oceanic crust (Vilà *et al.* 2010). The heat production in the lithospheric mantle is considered as null because of its very low content in radiogenic elements.

Fullea *et al.* (2007) performed a sensitivity analysis for the calculation of CMB and LAB depths induced by the typical root mean square (rms) error of elevation and geoid anomaly databases. They found that the inaccuracy for the crustal thickness in emerged regions is less than 2 km, whereas maximum error in lithospheric thickness is less than 10 km. The effect of varying crustal and lithospheric mantle conductivity has been tested

Table 2. Parameters used in our modeling, as a function of the zones defined on the Figure 1

Parameter	Zone 1	Zone 2	Zone 3	Zone 4	Zone 5	Oceanic crust
Crustal density at surface (kg m ⁻³)	[2608–2700]	[2605–2700]	[2601–2700]	[2605–2700]	[2601–2700]	[2602–2700]
Crustal density at CMB (kg m ⁻³)	2910	2910	2970	2910	2910	2980
Crustal radiogenic heat production ($\mu\text{W m}^{-3}$)	0.5	0.5	0.5	0.5	0.5	0.3

and the resulting lithospheric thickness is affected by up to 6–8 km, whereas varying the coefficient of thermal expansion (α) affects the lithospheric thickness by up to about 12 km. In addition, the crustal thickness is not much affected (*c.* 1 km) by varying thermal parameters.

Considering this sensitivity analysis, we estimated the maximum misfits obtained in our modelling result to be up to 5 km for the crustal thickness and up to 15 km for the lithospheric thickness.

Input data

Topography and bathymetry. Topographical and bathymetric data are extracted from the ETOPO1 database (Amante & Eakins 2009) (Fig. 3a). The most remarkable geomorphological feature of Central Eurasia is the Tibetan Plateau, which covers an area of more than 2.5×10^6 km² and has a mean elevation of around 4500 m. High elevations are also found to the north of the Tibetan Plateau, along the Tien Shan or the Qilian Shan ranges. The Tarim Basin presents a low relief with a mean elevation of around 1000 m. To the west, the highest elevations are located in the Zagros Mountains and they extend towards the Anatolian Plateau. The Alborz, Kopet Dagh, Caucasus and Sistan ranges also show remarkable topographies, with elevations of up to 5000 m. To avoid unrealistic high-frequency variations of the Moho and LAB depths, we have filtered the elevation using a Gaussian filter with a wavelength of 100 km.

Geoid anomaly. The geoid anomaly was extracted from the EGM2008 global model (Pavlis *et al.* 2008). The EGM2008 gravitational model is complete to spherical harmonic degree and order 2159, which determines the resolution of our modelling at 10 arc-min (*c.* 18.5 km). In order to avoid the effects of sublithospheric density variations, the geoid was filtered to remove the signature corresponding to the lower spherical harmonics until degree and order 11 (Fig. 3b). The degree and order of spherical harmonics filtering have been chosen in order to remove very large wavelength anomalies that probably result in sublithospheric density variations.

The obtained geoid anomaly shows maximum values of up to 21 m located in two main regions: (1) along the Himalaya and the Tibetan Plateau with a northward decrease of the anomaly; and (2) in the Anatolian Plateau, in the Alborz and in the Sanandaj–Sirjan zones in Iran. Minimum values are down to –21.5 m, coinciding with large sedimentary accumulations that occur in the Tarim, Junggar and Ganga basins, the Caspian Sea, the Nile delta, the Persian Gulf and eastern part of Arabia.

Comparison with seismological and seismic studies

We carried out a complete compilation of previously published crustal thickness data (Fig. 4, Table 3) mainly from receiver function and deep seismic studies. To test the reliability of our modelling approach, we compared this compilation to crustal thicknesses obtained from our modelling (Figs 5–7). The resulting CMB and LAB from our modelling approach are downloadable and are furnished in .txt format. In contrast to the CMB, the LAB corresponds to a rheological rather than to a compositional contrast, which explains why its location and properties are more elusive (Eaton *et al.* 2009). A shear-wave velocity anomaly within the upper mantle computed from global or regional tomography is often considered as correlated with the lithospheric thickness. We compare our results with the S40RTS mantle shear-wave velocity model (Ritsema *et al.* 2011). The LAB is rarely imaged using receiver function methods but we compared our modelling results with estimations from these studies where they were available (*e.g.* Kumar *et al.* 2007; Zhao *et al.* 2011).

The Arabian Plate

The crustal thickness of the Arabian Plate estimated from receiver functions, seismic refraction profiles and surface wave studies (see references in Table 3) ranges between 32 and 50 km, with an average value of around 40 km, which is consistent with our modelling results (Fig. 5a). Our map shows a smooth crustal thinning towards the NE of the Arabian Plate, which could be interpreted as inherited from the passive margin structure, although it is not well imaged by the scarce available seismic data. Both previous seismic studies and our modelling results image an abrupt crustal thinning along the boundaries of the Arabian Plate (the Gulf of Aden to the SE, the Gulf of Aqaba to the NW and the Red Sea to the west). Finally, beneath Oman and along the southern part of Red Sea coast, our model indicates that the crustal thickness may reach up to 43 km, whereas Al-Damegh *et al.* (2005) propose a crustal thickness of up to 50 km.

The shear-wave velocity anomaly map at a depth of 100 km shows a large low-velocity anomaly in western Arabia and along the Red Sea, whereas a positive anomaly is imaged beneath the Mesopotamian Basin (Villaseñor *et al.* 2001; Ritsema *et al.* 2011). Our model exhibits a thicker lithosphere in the eastern part of the Arabian Plate than to the western part, with a maximum thickness exceeding 200–220 km beneath the Persian Gulf and SE Arabia (Fig. 5b), which is in

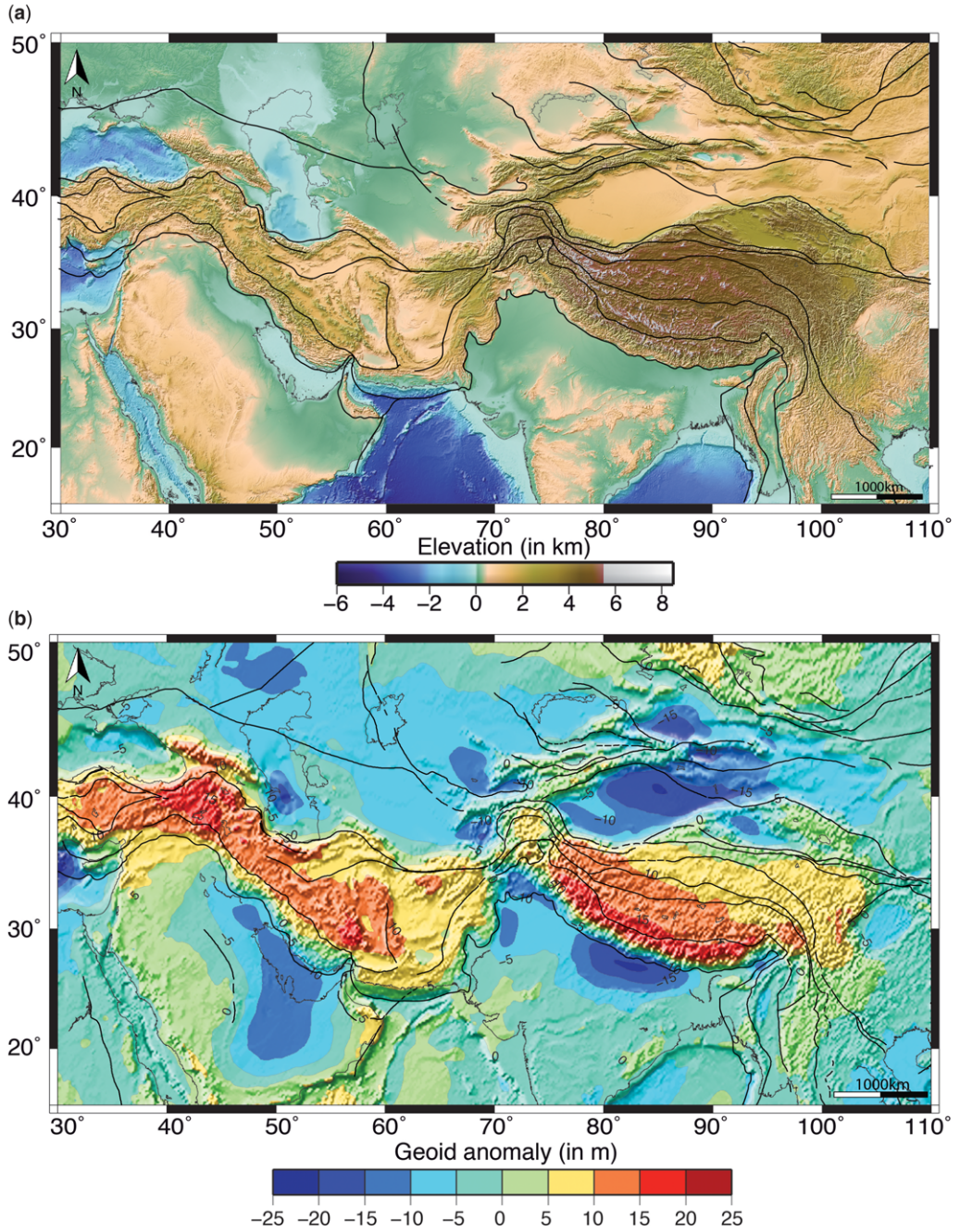


Fig. 3. (a) Elevation map from the ETOPO1 database (Amante & Eakins 2009). (b) Residual geoid height map resulting from the EGM2008 global model (Pavlis *et al.* 2008) after removing the lower spherical harmonics until degree and order 11. Main suture zones have been represented.

agreement with estimations from tomographical results (Villaseñor *et al.* 2001; Shomali *et al.* 2011). According to our results, this thickened lithosphere

extends beneath the Zagros Belt, which is also confirmed by shear-wave modelling (Priestley *et al.* 2012). Finally, our model indicates that towards

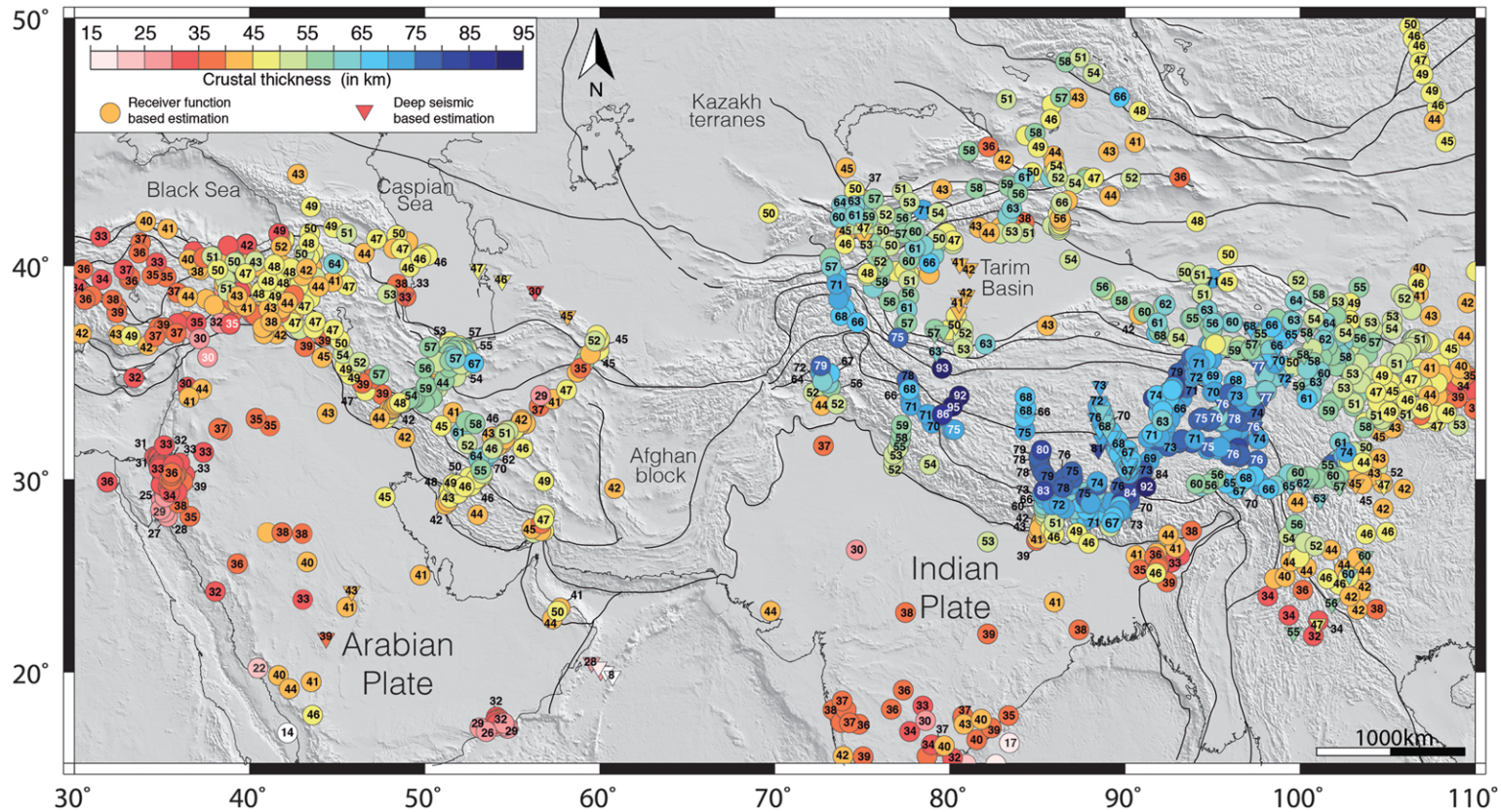


Fig. 4. Compilation of previous crustal thickness estimations from seismological and seismic experiments (complete references in Table 3).

Table 3. List of publications used for the compilation of crustal thickness data that are represented in Figure 4

Zone	References
Zone 1: Arabian Plate	Barton <i>et al.</i> (1990), Badri (1991), Sandvol <i>et al.</i> (1998), Kumar <i>et al.</i> (2001), Brew (2001), Al-Lazki (2003), Al-Damegh <i>et al.</i> (2005), Mohsen <i>et al.</i> (2006), Tiberi <i>et al.</i> (2007), Gök <i>et al.</i> (2008)
Zone 2: Indian Plate	Kumar <i>et al.</i> (2001, 2004, 2007), Gupta <i>et al.</i> (2003), Mitra <i>et al.</i> (2005, 2008), Radhakrishna <i>et al.</i> (2012)
Zone 3: Arabia–Eurasia collision zone	Mangino & Priestley (1998), Sandvol <i>et al.</i> (1998), Çakir <i>et al.</i> (2000), Brew (2001), Doloei & Roberts (2003), Zor <i>et al.</i> (2003), Al-Damegh <i>et al.</i> (2005), Angus <i>et al.</i> (2006), Paul <i>et al.</i> (2006, 2010), Nowrouzi <i>et al.</i> (2007), Gök <i>et al.</i> (2008, 2011), Gritto <i>et al.</i> (2008), Mellors <i>et al.</i> (2008), Nasrabadi <i>et al.</i> (2008), Sodoudi <i>et al.</i> (2009), Radjaee <i>et al.</i> (2010), Asfari <i>et al.</i> (2011), Motaghi <i>et al.</i> (2012), Yaminifard <i>et al.</i> (2012), Tezel <i>et al.</i> (2013)
Zone 4: India–Eurasia collision zone	Bump & Sheehan (1998), Kao <i>et al.</i> (2001), Li <i>et al.</i> (2001, 2008), Zhao <i>et al.</i> (2001, 2003, 2006), Galvé <i>et al.</i> (2002), Kind <i>et al.</i> (2002), Qiusheng <i>et al.</i> (2002), Vergne <i>et al.</i> (2002), Wang <i>et al.</i> (2003, 2010), Ross <i>et al.</i> (2004), Shi <i>et al.</i> (2004, 2009), Vinnik <i>et al.</i> (2004), Wittlinger <i>et al.</i> (2004), Kumar <i>et al.</i> (2005), Mi <i>et al.</i> (2005), Mitra <i>et al.</i> (2005, 2008), Schulte-Peklum <i>et al.</i> (2005), Tian <i>et al.</i> (2005), Jiang <i>et al.</i> (2006), Hetényi (2007), Tong <i>et al.</i> (2007), Oreshin <i>et al.</i> (2008), Li & Mashele (2009), Lou <i>et al.</i> (2009), Nabelek <i>et al.</i> (2009), Soomro (2009), Zhang & Wang (2009), Chen <i>et al.</i> (2010), Makarov <i>et al.</i> (2010), Robert <i>et al.</i> (2010a, b), Pan & Niu (2011), Tilmann (2011), Mechie <i>et al.</i> (2012), Yue <i>et al.</i> (2012), Gao <i>et al.</i> (2013), Xu <i>et al.</i> (2013), He <i>et al.</i> (2014)
Zone 5: North of the Tethysides	Mangino & Priestley (1998), Zorin <i>et al.</i> (2002), Zhao <i>et al.</i> (2003), Vinnik <i>et al.</i> (2004), Wang <i>et al.</i> (2004), Mellors <i>et al.</i> (2008), Chen <i>et al.</i> (2010), Radjaee <i>et al.</i> (2010), Pan & Niu (2011), Motaghi <i>et al.</i> (2012)

the NW of the Mesopotamian Basin, the lithosphere thickness decreases and reaches minimum values of about 140 km south of the Anatolian Plateau.

The Indian Plate

Previous crustal thickness estimations of the Indian Plate vary from 30 to 44 km but most of these estimations are comprised between 36 and 39 km (see references in Table 3). Our modelling results fit very well with previously obtained crustal thicknesses for the whole Indian Plate, except for the Shillong Plateau where our model predicts a thicker crust due to the fact that our approach is not strictly valid to image an uncompensated crustal pop-up structure, as proposed by Mitra *et al.* (2005).

Previous studies using surface-wave-dispersion data observed a shield-like lithospheric structure in most parts of the plate (Singh 1999; Mitra *et al.* 2006; Suresh *et al.* 2008; Bhattacharya 2009; Prajapati *et al.* 2011) and there are no major lateral variations in the shear-wave velocity anomalies across the Indian Plate (Villaseñor *et al.* 2001; Ritsema *et al.* 2011). According to previous geophysical studies, the lithospheric thickness beneath western India is around 155 km (Mitra *et al.* 2006) and about 140 km beneath eastern India (Bhattacharya

2009). Our model images an approximately 160–190 km-thick lithosphere; although a lithosphere thickness reaching up to 230 km is imaged below the central part of the Ganga Basin (Fig. 5b). In this region, the possible component of flexural support to the lithospheric bending, evidenced by large sedimentary thickness accumulation, could also affect the validity of our approach and result in an overestimation of our modelled lithospheric thickness. However, the lack of other geophysical data in this area does not allow for firm conclusions.

The Arabia–Eurasia collision zone

In agreement to previous geophysical studies, our modelling results show crustal thickness values ranging between 35 and 45 km beneath the Mesopotamian Basin (see the references in Table 3). Along the Zagros Orogeny, seismic data indicate that the maximum crustal thickness is located below the Sanandaj–Sirjan Zone, whereas our model predicts the maximum crustal thickness values slightly displaced to the SW, coinciding with the highest elevations and directly below the Imbricated Zone and the Zagros Simply Folded Belt (Fig. 5a). This shift of the maximum crustal root relative to maximum topography is common in collisional settings where crustal thickening is associated with

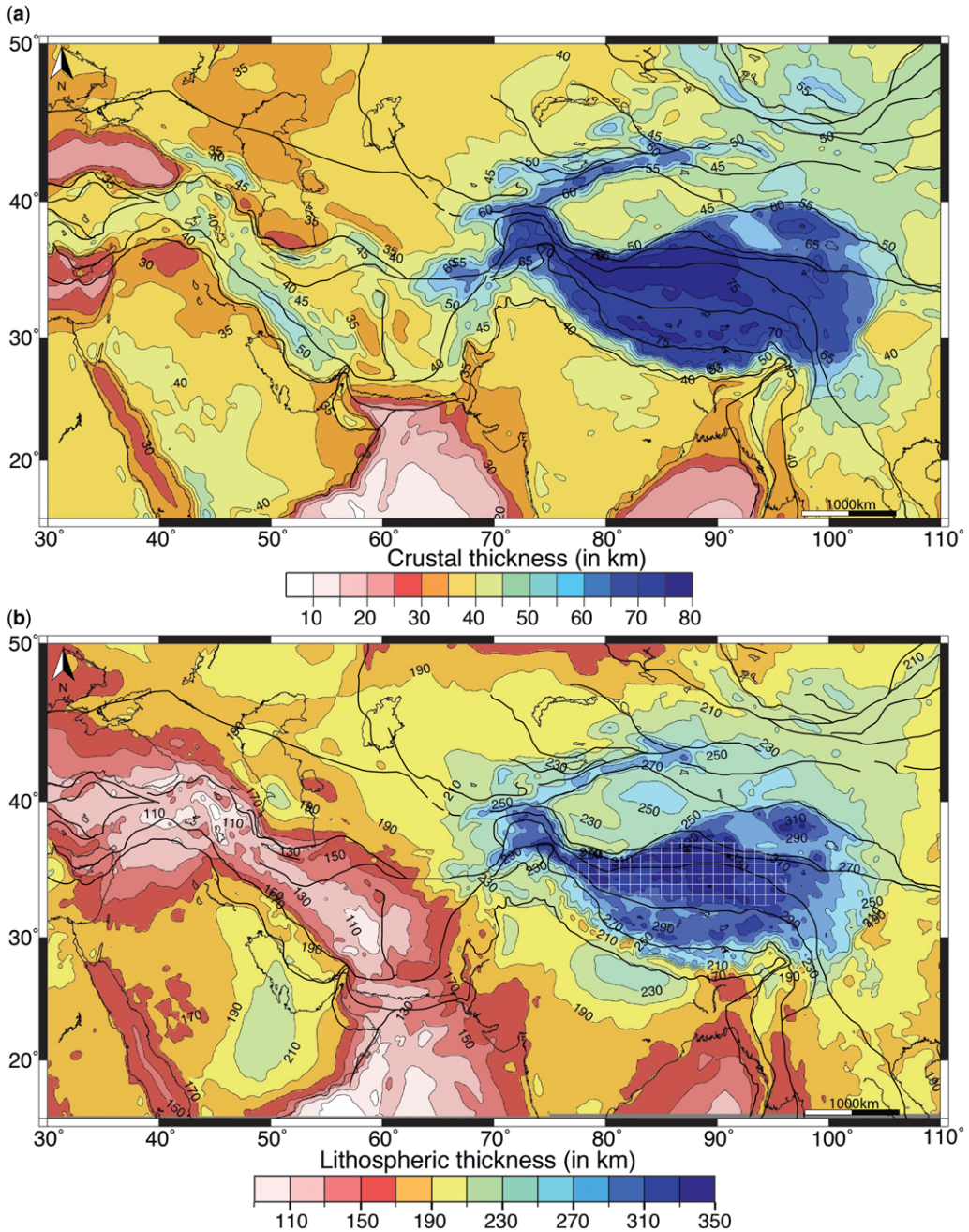


Fig. 5. (a) Crustal thickness map and (b) lithospheric thickness map of the entire Central Eurasia region calculated from elevation and geoid anomaly inversion. The hatched zone denotes the region where our model is not able to discern the lithospheric structure.

underthrusting or down-flexuring at the crustal scale, as might be the case for the Zagros Orogeny (Motavalli-Anbaran *et al.* 2011; Vergés *et al.*

2011). Our 1D approach, based on the combination of elevation and geoid anomaly, is not able to reproduce these underthrusting structures and

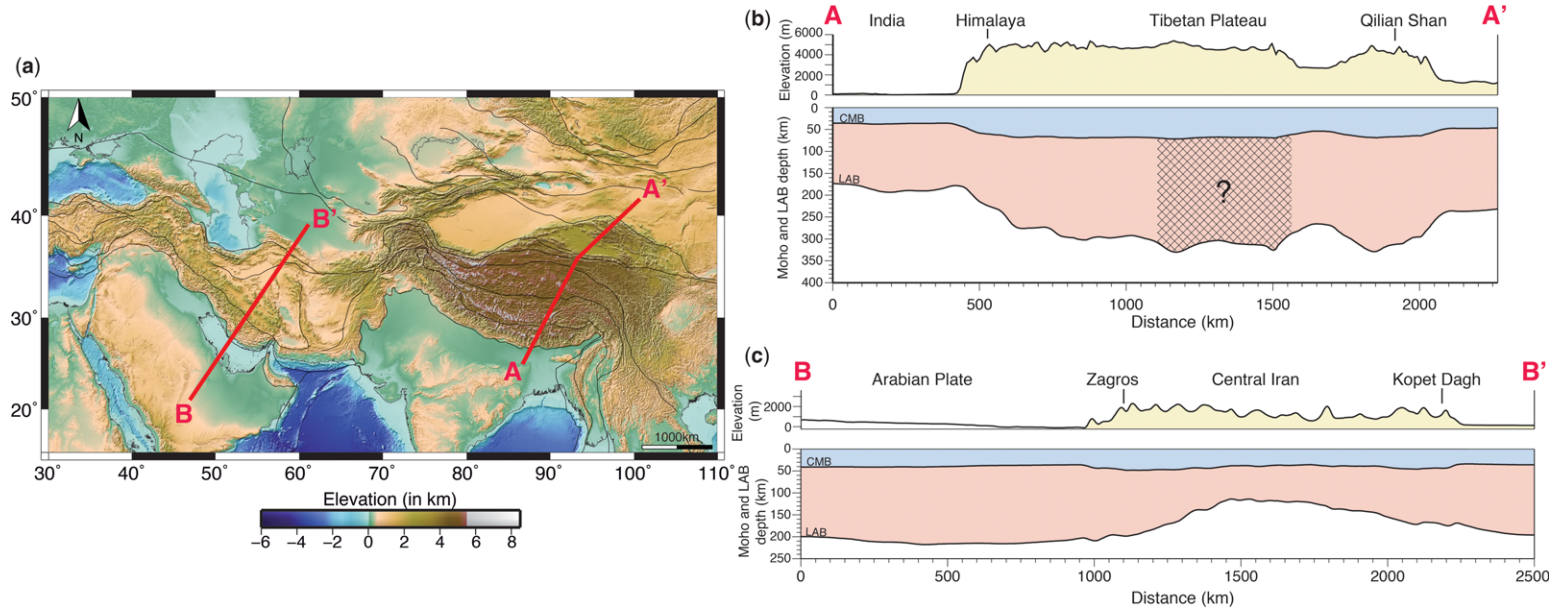


Fig. 6. (a) Topographical map of the study region and the location of two lithospheric cross-sections. (b) Lithospheric cross-section across the India–Eurasia collision zone representing the topography and the depths of the crust–mantle boundary (CMB) and the lithosphere–asthenosphere boundary (LAB). (c) Same as (b) but across the Arabia–Eurasia collision zone.

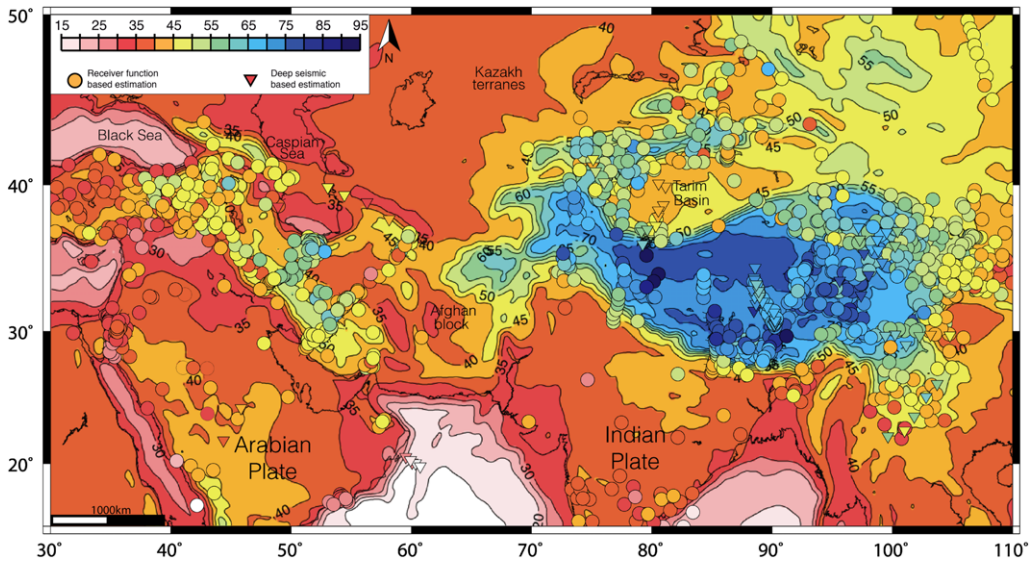


Fig. 7. Comparison between crustal thickness estimations from seismological and seismic experiments (circles and triangles corresponding to Fig. 4) and the calculated values from the inversion of geoid and elevation (background map corresponding to Fig. 5a). Similar colours between filled symbols and the background map indicate the coincidence between seismic data and the model results.

therefore to precisely locate the region with maximum crustal thickness. However, our modelling results indicate crustal thickness values of between 35 and 54 km beneath the Iranian and Afghan blocks, in good agreement with available seismic data in Central Iran (Paul *et al.* 2006, 2010; Nasrabadi *et al.* 2008; Asfari *et al.* 2011; Motaghi *et al.* 2012) and suggesting that the stiff lithospheric domains are related to relatively low crustal thickness values. The Alborz, Kopet Dagh and Caucasus mountain ranges are characterized by thickened crust according to both seismic data and modelling results (Fig. 7). In the Anatolian Plateau, our model shows crustal thickness values of between 36 and 50 km, in good agreement with most of the estimations from seismological studies, which in turn show a large scattering (up to *c.* 20 km in difference).

Shear-wave velocity studies in the Arabia–Eurasia collision zone show a thick high shear-wave velocity anomaly within the upper mantle beneath eastern Arabia and Zagros, whereas western Arabia, Central Iran and the Anatolian Plateau domains are characterized by low shear-wave velocity anomalies within the upper mantle (Villaseñor *et al.* 2001; Priestley *et al.* 2012). Low shear-wave velocities underneath the eastern part of the Anatolian Plateau are interpreted as a consequence of a very thin or possibly removed lithospheric mantle (Gök *et al.* 2008; Bakirci *et al.* 2012), which is confirmed by S-receiver functions studies (Angus

et al. 2006) and low Pn wave speeds (Al-Lazki *et al.* 2004). Mohsen *et al.* (2006) proposed a lithospheric thickness value of 90 km beneath eastern Anatolia, which is in agreement with our model, highlighting a thin lithosphere beneath the whole Anatolian Plateau (from 100 to 130 km thick).

The India–Eurasia collision zone

Many geophysical studies have been carried out across the Himalayan range and the Tibetan Plateau to image its complex crustal and lithospheric structure. Most of these studies are based on deep seismic profiles (Zhao *et al.* 2001, 2006; Galvé *et al.* 2002; Ross *et al.* 2004; Mechie *et al.* 2012) and on passive seismological data (see the whole set of references in Table 3). A general result is that, despite its low relief and high elevation, the Tibetan Plateau shows a highly variable crustal thickness ranging from 56 up to 95 km and a heterogeneous lithospheric structure (e.g. Yin & Harrison 2000; Zhao *et al.* 2010). Collectively, the results suggest that the crust is thicker in the southern part (between 70 and 80 km thick) of the plateau than to the north (between 65 and 70 km thick) except for the easternmost part of the plateau (longitude >95°E). In contrast, our results indicate that the crust in the southern part of the Tibetan Plateau ranges between 68 and 76 km thick, whereas it predicts a thicker crust (more than 75 km thick) in the northern part of the plateau (Fig. 5a). To the

west of the Tibetan Plateau, seismological studies indicate a noticeable crustal thickening from approximately 50 km below the front of the Himalayan range in Pakistan (Soomro 2009) to around 78 km below the Pamir (Li & Mashele 2009; Mechie *et al.* 2012). Our model is broadly in agreement with these estimations, although it slightly underestimates the crustal thickness below southern Pamir.

Our model is able to reproduce the lithospheric thickness in the southern and western part of the plateau, in agreement with receiver function data (Owens & Zandt 1997; Nabelek *et al.* 2009; Zhao *et al.* 2010, 2011), tomographic data (Villaseñor *et al.* 2001; Priestley *et al.* 2006; Replumaz *et al.* 2013) and previous lithospheric modelling (Jiménez-Munt *et al.* 2008) that suggest an approximately 200–240 km-thick lithosphere. Most authors agree that this thick Tibetan lithosphere corresponds to the northern boundary of the underthrust Indian lithosphere below Tibet (e.g. Owens & Zandt 1997; Nabelek *et al.* 2009; Zhao *et al.* 2010, 2011; Liang *et al.* 2012). The main discrepancy concerns the northern part of the Tibetan Plateau, where some studies suggest a very thin to non-existent lithospheric mantle (e.g. Meissner *et al.* 2004; Jiménez-Munt *et al.* 2008; Liang *et al.* 2012), whereas other studies suggest a very thick lithosphere (e.g. Priestley *et al.* 2006; Barron & Priestley 2009). Our model results indicate a very thick lithosphere, up to 340 km in thickness, coinciding with the region where our model overestimates the crustal thickness. However, using the same geoid and elevation data plus gravity and thermal data, Jiménez-Munt *et al.* (2008) proposed a very thin to removed lithosphere. Unfortunately, our results do not allow any differentiation between the proposed geodynamic processes acting in this peculiar part of the Tibetan Plateau.

North of the Tethysides

According to seismological and seismic studies, the Tarim Basin is characterized by a crustal thickness of about 40 km in its central part, increasing up to around 60 km in its flanks (Kao *et al.* 2001; Qiusheng *et al.* 2002; Zhao *et al.* 2003, 2006; Wittlinger *et al.* 2004; Mi *et al.* 2005; Chen *et al.* 2010). Our model overestimates by approximately 5 km the crustal thickness in the Central Tarim Basin and does not reflect noticeable crustal thickness variations beneath the basin (Fig. 5a). According to seismological estimations, the crustal thickness below the Tien Shan is 55–60 km (Bump & Sheehan 1998; Zhao *et al.* 2003; Vinnik *et al.* 2004), whereas our model predicts crustal thickness values of between 60 and 68 km. In the Kazakh terranes, NW from Tien Shan, the small

number of available seismological estimations indicate a crustal thickness of about 45 km (Bump & Sheehan 1998; Vinnik *et al.* 2004), which is very close to the 40–44 km obtained from our model for the whole region. In the NE part of the study area, north of the Altaids Ranges, the crustal thickness inferred from receiver functions (Zorin *et al.* 2002) varies from 44 to 50 km in full agreement with our results.

The lithospheric thickness have been estimated from S-wave receiver functions (Kumar *et al.* 2005) indicating values of 90–120 km beneath the Tien Shan, around 180 km in the Tarim Basin and about 130 km in the Kazakh Platform. Our results show a thicker lithosphere in all of these regions, varying from 240 km in the Tien Shan, to 220 km in the Tarim Basin and 180 km in the Kazakh Platform, being in agreement with S-wave tomography models, which indicate high velocities below the Tien Shan and the Tarim basin (Ritsema *et al.* 2011).

Discussion

One of the goals of the present study is to provide new maps of both the crust–mantle boundary and the lithosphere–asthenosphere boundary in the Central Eurasia region, and to compare these results with previous regional/global models. A second related goal is to discuss the implications on the geodynamic evolution of this large continental collision region based on our crustal and lithospheric thickness maps.

Our modelling approach is based on the assumptions of local lithospheric isostasy and thermal equilibrium. Whereas local isostasy is an acceptable approximation for wavelengths of hundreds of kilometres (e.g. McKenzie & Bowin 1976; England & Molnar 1997), the assumption of thermal equilibrium is not valid in regions of recent tectonic activity, such as the Alpine–Himalayan system. Therefore, the results of our model must be interpreted as average physical conditions necessary to produce the required density distribution rather than the actual thermal boundaries. The calculation in steady state minimizes the variations in lithospheric thickness, since the modelling tends to underestimate the lithosphere thickness when the thickening processes occur under transient conditions, and overestimate it for thinning processes (see Fullea *et al.* 2007; Jiménez-Munt *et al.* 2011 for more details).

Comparison with global crustal models

The most widely used global datasets related to crustal thickness is the CRUST2.0 (Bassin *et al.*

2000), which has recently been replaced by the CRUST1.0 that incorporates an updated version of global sediment thickness and presents a better accuracy (Laske *et al.* 2013). Reguzzoni *et al.* (2013) combined CRUST2.0 model with gravity observations from the GOCE satellite to propose the new global crustal GEMMA model that we compare with our results (Fig. 7).

The $1^\circ \times 1^\circ$ grid global crustal model CRUST1.0 is obtained from the analysis of seismic wave travel-times and seismic refraction data (Laske *et al.* 2013). The resulting crustal thickness from the CRUST1.0 model (Fig. 8a) in the study region is relatively smooth, with maximum values exceeding 70 km in the Tibetan Plateau, and minimum values of <15 km in the oceanic domains of the Red Sea and the Indian Ocean. Most of the continental domains show crustal thickness values of 40 ± 5 km. The excessive smoothness of the resulting map makes it difficult to relate crustal thickness variations with surface geological structures. Therefore, the crustal thickness derived from our model exceeds that from CRUST1.0 by more than 10–15 km along the main mountain ranges (i.e. Red Sea rift shoulders, Anatolia, Caucasus, Zagros, Alborz, Makran, Pamir, Qiangtang and Tien Shan).

The resulting crustal thickness from the GEMMA Moho model (Reguzzoni *et al.* 2013) ranges from 15 to more than 100 km and presents large undulations of around 40 km over the whole region (Fig. 8b). In contrast, our method allows for a better interpolation between regions with reliable measurements and then show a much better correlation with the major geological structures (Fig. 8c).

Comparison with global lithospheric models

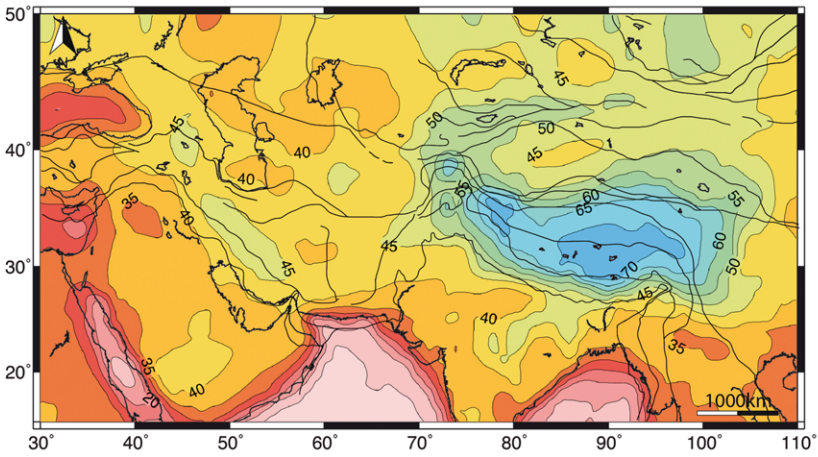
Concerning the lithospheric thickness, we compare our modelling results with two lithospheric models: the TC1 model (Artemieva 2006) (Fig. 9) and the thermal lithospheric model presented in Goutorbe *et al.* (2011). In addition to these two models, there are a number of regional/global seismic tomography models and several regional studies based on the combination of different geological and geophysical data that can also constrain the crust and upper-mantle structures as compared below.

The resulting lithospheric thickness from our model can be qualitatively compared to regional/global models based on seismic surface waves and thermal approaches. Regional and global S-wave velocity perturbations in the Central Eurasia region at a depth of 100 km (e.g. Villaseñor *et al.* 2001; Priestley *et al.* 2006; Hatzfeld & Molnar 2010; Ritsema *et al.* 2011 and references therein) show

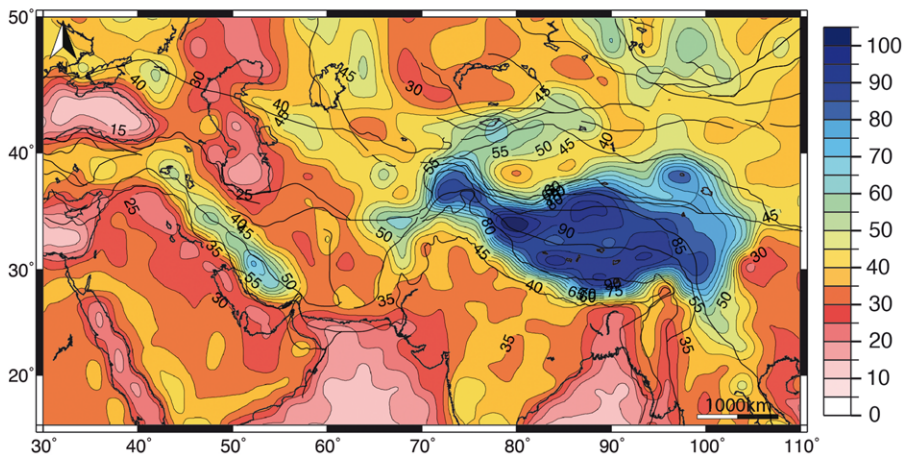
low velocities beneath the Red Sea, Eastern Anatolia, Central Iran and Afghan blocks, Eastern Tibet, and north to the Altaid ranges, with some differences between these models. High-velocity perturbations are located beneath north India and West Tibet, and in northern regions. Major differences between our model and S-wave tomography models are related to the lateral variations in lithospheric thickness from the Zagros to Central Iran and the Mesopotamian Basin. Some tomography models (e.g. Priestley *et al.* 2006, 2012) propose a lithosphere thickness exceeding 230 km along the so-called Zagros core, thinning rapidly towards Central Iran and the Mesopotamian Basin. In contrast, our model shows that the thick lithosphere affects the Mesopotamian Basin, the SE Arabian Plate and the Zagros up until the Arabia–Eurasia continental suture, with an abrupt thinning beneath the Sanandaj–Sirjan Zone and the Urumieh–Doktar Magmatic Arc. This lithosphere thinning extends from Anatolia, to Central Iran and to the Afghan block, which is more in agreement with the tomography models by Villaseñor *et al.* (2001) and Ritsema *et al.* (2011) that also show a lithospheric thickening beneath the Mesopotamian Basin as in our model. Another conflictive region is Eastern Tibet, where all tomography models show a relatively low-velocity region at a depth of 100–125 km, vanishing with depth and then disappearing at 200 km depth. Finally, the high-velocity anomalies occupying most of the northern regions of the study area are in agreement with the lithospheric thickness of 170–200 km proposed by our model. This fitting is not accomplished north of the Altaid ranges where tomography models consistently image a low-velocity region in contrast to a somewhat homogeneous lithospheric thickness of 180–200 km inferred from our calculations. In any case, the interpretation of S-wave tomography in terms of thermal models must take into account that velocity anomalies of non-thermal origin may amount up to $\pm 3\%$ of V_s amplitude and be attributed to chemical composition variations and/or to the presence of melts/fluids (Artemieva 2009).

Global thermal models can be directly compared to our results since the approach used in the present work includes thermal analysis. TC1 is a global-scale continental lithospheric model that has been computed from available heat-flow measurements supplemented with electromagnetic and xenolith data in cratonic domains (Artemieva 2006) (Fig. 8a). In Central Eurasia, the TC1 model proposes a lithospheric thickness ranging from less than 100 km below Anatolia and Iran, up to more than 200 km in the NE Tibetan Plateau and west-central part of the Indian Plate. Our model presents a roughly similar trend to the distribution of the

(a) Crustal thickness (in km) from CRUST 1.0 model



(b) Crustal thickness (in km) from GEMMA crustal model



(c) Crustal thickness (in km) from our modelling

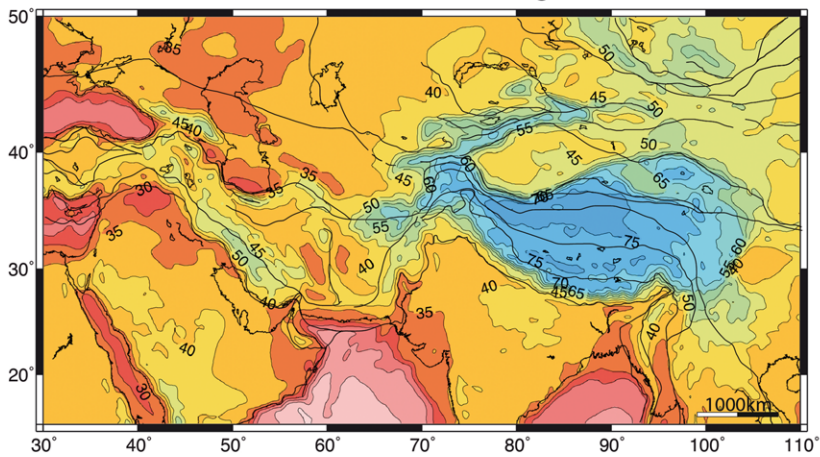
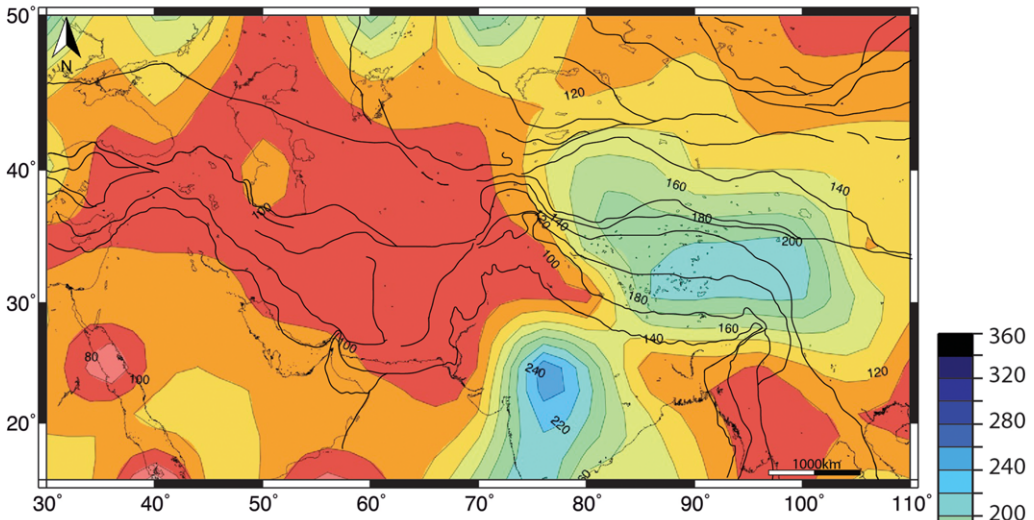


Fig. 8. Crustal thickness maps from (a) the CRUST 1.0 model (1° grid resolution) (Bassin *et al.* 2000), (b) the GEMMA Moho model (Reguzzoni *et al.* 2013) and (c) our results (0.16° grid resolution). Major sutures zones are plotted.

(a) Lithospheric thickness (in km) from TC1 thermal model



(b) Lithospheric thickness (in km) from our modeling

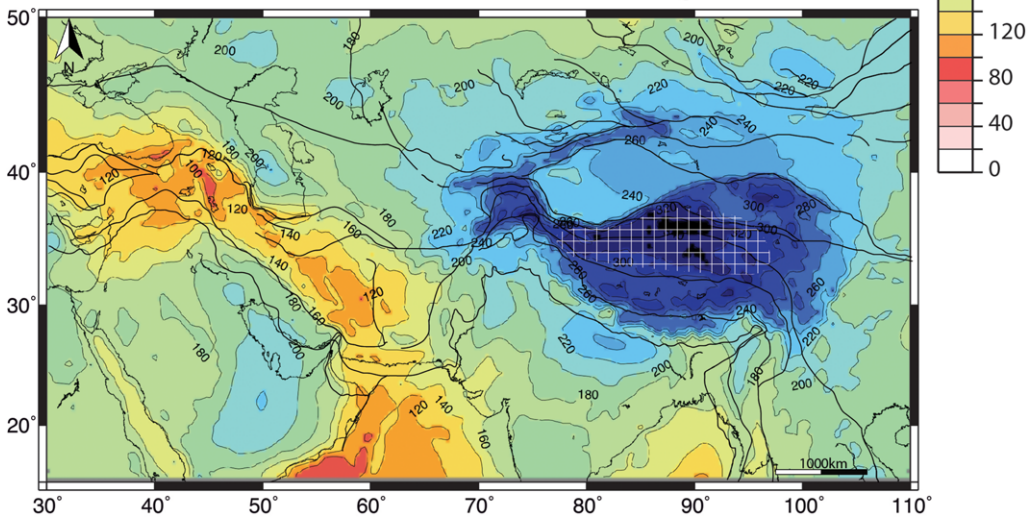


Fig. 9. Lithospheric thickness maps from (a) the TC1 thermal model (Artemieva 2006) and (b) from our results. Major sutures zones are plotted. The hatched zone denotes the region where our model is not able to discern the lithospheric structure.

lithospheric thickness but with a higher resolution and more precise lithospheric thickness estimations in the study region (Fig. 8b). The lithospheric thickening affecting the eastern Arabian Plate and the Mesopotamian Basin, as well as the Tibetan Plateau and the North India Plate. Lithospheric thinning is concentrated along the Red Sea and its shoulders, Anatolia, and the Central Iran and Afghan blocks. Goutorbe *et al.* (2011) published a thermal model obtained from heat-flow measurements combined with multiple geological and geophysical

data and proxies. This model reproduces the lithospheric thickening affecting the eastern Arabian Plate and the Mesopotamian Basin, as well as the Tibetan Plateau and the North India Plate. Lithospheric thinning is concentrated along the Red Sea and its shoulders, Anatolia, and the Central Iran and Afghan blocks. The proposed lithospheric thickness values are, however, unrealistically low, especially in the thinned regions, where the LAB is less than 40 km thick.

Geodynamic implications

The new results indicate that crustal thickening in Central Eurasia is clearly associated with major frontal ranges, such as the Himalaya and Zagros, but also with distal ranges, such as the Alborz, Kopet Dagh and Tien Shan. The more than 1200 km in width of the deformed area resulting from the Arabia–Eurasia and India–Eurasia collision zones is also highlighted by the extent of the area affected by crustal thickening (Figs 1 & 5a). As already suggested by many geophysical studies, the Tibetan Plateau is sustained by a very thick crust with an average thickness of around 75 km according to our model. Furthermore, the tectonic blocks remaining in the deformation zone, as the Central Iran or Tarim blocks, show a slightly thickened crust and uniform topography pointing out their rheological resistance and moderate deformation. A consequence of these features is that tectonic stresses can be efficiently transmitted for hundreds to thousands of kilometres from the suture zones.

Contrary to the crustal structures that are comparable between the two collision zones, their lithospheric structures differ substantially (Figs 5 & 6). The Arabia–Eurasia collision zone is characterized by a thick lithosphere underneath the Zagros Belt and the Arabian Platform (between 180 and 220 km thick), whereas Central Iran, the Anatolian Plateau and the northern part of the Arabian Plate are characterized by thin to very thin lithosphere (90–150 km in thickness). In contrast, the India–Eurasia collision zone shows a thick to very thick lithosphere, especially in its southern part, thus evidencing the plate underthrusting of most part of the Indian lithosphere beneath the Eurasian lithosphere. The large differences in lateral thickness variations between the crustal and the lithospheric mantle indicate a strong strain partitioning, with the CMB acting as the preferential detachment level as proved in Iran (Jiménez-Munt *et al.* 2012).

Conclusions

We present a new crustal and lithospheric thickness model assuming thermal and isostatic equilibrium that fits well with existing seismic and seismological data. The method used allows crustal and lithospheric thickness values to be interpolated between regions with reliable measurements, and provides a full coverage for both the crust and the lithosphere of Central Eurasia. The presented work allows the following concluding remarks to be made:

- Crustal thickening is correlated with major mountains ranges (Himalayas, Zagros, Pamir, Caucasus and Tien Shan), whereas crustal

thinning is restricted to the Arabian and Indian oceanic domains, and to the South Caspian Sea, the Red Sea and the Black Sea. The Iranian and Anatolian plateaus do not show a significant thick crust, whereas the Tibetan Plateau shows an extremely thickened crust up to 78 km thick. At a regional scale, our resulting map matches well with geological features.

- Contrasting lithospheric structures are modelled between the India–Eurasia and the Arabia–Eurasia collision zones. Thickened lithosphere is obtained below the Zagros orogenic belt, whereas the Anatolian Plateau and Central Iran are characterized by a thin to very thin lithosphere (*c.* 100–130 km thick). In contrast, maximum lithospheric thickness, reaching up to 300 km, corresponds to the southern and western Tibetan Plateau and below the Pamir. Our model coincides well with S-wave tomography models but not in Eastern Tibet where our model cannot resolve the existence of a Low-Velocity Zone down to 200 km depth, suggesting a lithospheric thinning related to deep geodynamic processes.
- Our resulting crustal map is roughly in good agreement with the global CRUST1.0 and GEMMA Moho models. However, the crustal thickness derived from our model exceeds that from CRUST1.0 by more than 10–15 km along the main mountain ranges, which better fits the crustal thickness in these tectonic domains based on geophysical studies. Our resulting model presents a similar trend of the distribution of the lithospheric thickness compared to regional and global models but it also presents better resolution and thickness estimations.
- India–Eurasia and Arabia–Eurasia collisional systems present comparable crustal structure but contrasted lithospheric structure. The Arabia–Eurasia collision zone is characterized by a very thin lithosphere that can be interpreted as the signature of the dominance of subduction processes. Oppositely, the more mature India–Eurasia collision zone shows a thick lithosphere in its western and central parts that highlights the importance of crustal underthrusting processes.
- Our new results indicate that crustal thickening is not restricted but, rather, extends hundreds to thousands of kilometres away from the collision front, indicating an effective transmission of tectonic stresses, which is partly related to the presence of stiff lithospheric blocks that remain almost undeformed within the collisional systems.

This research has been funded by DARIUS Consortium and projects ATIZA (CGL2009-09662-BTE), TECLA (CGL2009-09662-BTE) and Consolider-Ingénio 2010

Topo-Iberia (CSD2006-00041). Some figures were generated using GMT (Wessel & Smith 1991). The authors thank Alexander Koptev, Joerg Ebbing and Marie-Françoise Brunet for their constructive comments on the manuscript that helped to improve this article.

References

- AGARD, P., OMRANI, J. *ET AL.* 2011. Zagros orogeny: a subduction-dominated process. *Geological Magazine*, **148**, 692–725.
- AL-DAMEGH, K., SANDVOL, E., AL-LAZKI, A. A. & BARAZANGI, M. 2004. Regional seismic wave propagation (Lg and Sn) and Pn attenuation in the Arabian Plate and surrounding regions. *Geophysical Journal International*, **157**, 775–795.
- AL-DAMEGH, K., SANDVOL, E. & BARAZANGI, M. 2005. Crustal structure of the Arabian Plate: new constraints from the analysis of tele-seismic receiver functions. *Earth and Planetary Science Letters*, **231**, 177–196.
- AL-LAZKI, A. I. 2003. *Crustal and upper mantle structure of Oman and the northern Middle East*. PhD thesis, Cornell University.
- AL-LAZKI, A. I., SANDVOL, E., SEBER, D., BARAZANGI, M., TURKELLI, N. & MOHAMAD, R. 2004. Pn tomographic imaging of mantle lid velocity and anisotropy at the junction of the Arabian, Eurasian and African plates. *Geophysical Journal International*, **158**, 1024–2040.
- AMANTE, C. & EAKINS, B. W. 2009. *ETOPO1 1 Arc-minute Global Relief Model: Procedures, Data Sources and Analysis*. NOAA Technical Memorandum NESDIS NGDC-24.
- ANGUS, D. A., WILSON, D. C., SANDVOL, E. & NI, J. F. 2006. Lithospheric structure of the Arabian and Eurasian collision zone in Eastern Turkey from S-wave receiver functions. *Geophysical Journal International*, **166**, 1335–1346.
- ARTEMIEVA, I. M. 2006. Global $1^\circ \times 1^\circ$ thermal model tc1 for the continental lithosphere: implications for lithosphere secular evolution. *Tectonophysics*, **416**, 245–277.
- ARTEMIEVA, I. M. 2009. The continental lithosphere: reconciling thermal, seismic, and petrologic data. *Lithos*, **109**, 23–46.
- ASFARI, N., SODOUDI, F., FARAHMAND, F. T. & GHASSEMI, M. R. 2011. Crustal structure of northwest Zagros (Kermanshah) and Central Iran (Yazd and Isfahan) using teleseismic PS converted phases. *Journal of Seismology*, **15**, 341–353.
- AUDET, P. & BÜRGMANN, R. 2011. Dominant role of tectonic inheritance in supercontinent cycles. *Nature Geoscience*, **4**, 184–187.
- BADRI, M. 1991. Crustal structure of central Saudi Arabia determined from seismic refraction profiling. *Tectonophysics*, **185**, 357–374.
- BAKIRCI, T., YOSHIZAWA, K. & OZER, M. F. 2012. Three-dimensional S-wave structure of the upper mantle beneath Turkey from surface wave tomography. *Geophysical Journal International*, **190**, 1058–1076.
- BARRON, J. & PRIESTLEY, K. 2009. Observations of frequency-dependent Sn propagation in Northern Tibet. *Geophysical Journal International*, **179**, 475–488.
- BARTON, P. J., OWEN, T. R. E. & WHITE, R. S. 1990. The deep structure of the east Oman continental margin: preliminary results and interpretation. *Tectonophysics*, **173**, 319–331.
- BASSIN, C., LASKE, G. & MASTERS, G. 2000. The current limits of resolution for surface wave tomography in North America. *Eos, Transactions of the American Geophysical Union*, **81**, F897.
- BHATTACHARYA, S. N. 2009. Computation of surface wave velocities in an isotropic nongravitating spherical earth using an exact flattening transformation. *Bulletin of the Seismological Society of America*, **99**, 3525–3528.
- BREW, G. E. 2001. *Tectonic evolution of Syria interpreted from integrated geophysical and geological analysis*. PhD thesis, Cornell University.
- BRUNET, M.-F., KOROTAEV, M. V., ERSHOV, A. V. & NIKISHIN, A. M. 2003. The South Caspian Basin: a review of its evolution from subsidence modelling. *Sedimentary Geology*, **156**, 119–148.
- BUMP, H. A. & SHEEHAN, A. F. 1998. Crustal thickness variations across the northern Tien Shan from teleseismic receiver functions. *Geophysical Research Letters*, **25**, 1055–1058.
- ÇAKIR, O., ERDURAN, M., ÇINAR, H. & YILMAZTÜRK, A. 2000. Forward modelling receiver functions for crustal structure beneath station TBZ (Trabzon; Turkey). *Geophysical Journal International*, **140**, 341–356.
- CHEN, Y., NIU, F., LIU, R., HUANG, Z., TKALCIC, H., SUN, L. & CHAN, W. 2010. Crustal structure beneath China from receiver function analysis. *Journal of Geophysical Research: Solid Earth*, **115**, 2156–2202.
- CLAUSER, C. & HUENGES, E. 1995. Thermal conductivity of rocks and minerals. In: AHRENS, T. J. (ed.) *Rocks Physics & Phase Relations: A Handbook of Physical Constants*. American Geophysical Union, Washington, DC, 105–126, <https://doi.org/10.1029/RF003>
- DOLOEI, J. & ROBERTS, R. 2003. Crust and uppermost mantle structure of Tehran region from analysis of teleseismic P-waveform receiver functions. *Tectonophysics*, **364**, 115–133.
- EATON, D. W., DARBYSHIRE, F., EVANS, R. L., GRÜTTER, H., JONES, A. G. & YUAN, X. 2009. The elusive Lithosphere-Asthenosphere boundary (LAB) beneath cratons. *Lithos*, **109**, 1–22.
- ENGLAND, P. & MOLNAR, P. 1997. Active deformation of Asia: from kinematics to dynamics. *Science*, **278**, 647.
- EXXON 1994. *Exxon Tectonic Map of the World*. Exxon Production Research Company, 1985, prepared by the World Mapping Project as part of the Tectonic Map Series of the World. Exxon Production Research Company and World Mapping Project and American Association of Petroleum Geologists Foundation.
- FRIZON DE LAMOTTE, D., LETURMY, P., AGARD, P., RINGENBACH, J.-C., ROBERT, A., WROBEL-DAVREAU, C. & SHERKATI, S. 2013. Tectonic Map of the Arabian Plate and Surrounding Areas. Commission for the Geological Map of the World (CGMW), Paris.
- FULLEA, J., FERNÁNDEZ, M., ZEYEN, H. & VERGÉS, J. 2007. A rapid method to map the crustal and lithospheric thickness using elevation, geoid anomaly and

- thermal analysis. Application to the Gibraltar arc system, Atlas mountains and adjacent zones. *Tectonophysics*, **430**, 97–117.
- GALVÉ, A., SAPIN, M. *ET AL.* 2002. Complex images of Moho and variation of V_P/V_S across the Himalaya and South Tibet, from a joint receiver-function and wide-angle-reflection approach. *Geophysical Research Letters*, **29**, 35-1–35-4.
- GAO, R., CHEN, C., LU, Z., BROWN, L. D., XIONG, X., LI, W. & DENG, G. 2013. New constraints on crustal structure and Moho topography in Central Tibet revealed by SinoProbe deep seismic reflection profiling. *Tectonophysics*, **606**, 160–170.
- GÖK, R., MAHDI, H., AL-SHUKRI, H. & RODGERS, A. J. 2008. Crustal structure of Iraq from receiver functions and surface wave dispersion: implications for understanding the deformation history of the Arabian-Eurasian collision. *Geophysical Journal International*, **172**, 1179–1187.
- GÖK, R., MELLORS, R. J. *ET AL.* 2011. Lithospheric velocity structure of the Anatolian Plateau Caucasus–Caspian region. *Journal of Geophysical Research*, **116**, B05303.
- GOUTORBE, B., POORT, J., LUCAZEAU, F. & RAILLARD, S. 2011. Global heat flow trends resolved from multiple geological and geophysical proxies. *Geophysical Journal International*, **187**, 1405–1419.
- GRITTO, R., SIBOL, M. S. *ET AL.* 2008. *Crustal structure of North Iraq from receiver function analyses. Monitoring Research Review: Ground-based nuclear explosion monitoring technologies*. Contract No. FA8718-07-C-0008.
- GUPTA, S., RAI, S. S. *ET AL.* 2003. The nature of the crust in southern India: implications for Precambrian crustal evolution. *Geophysical Research Letters*, **30**, 1419.
- HATZFELD, D. & MOLNAR, P. 2010. Comparisons of the kinematics and deep structures of the Zagros and Himalaya and of the Iranian and Tibetan plateaus and geodynamic implications. *Reviews of Geophysics*, **48**, RG2005.
- HE, C., SANTOSH, M., CHEN, X. & LI, X. 2014. Crustal growth and tectonic evolution of the Tianshan orogenic belt, NW China: a receiver function analysis. *Journal of Geodynamics*, **75**, 41–52.
- HEARN, T. M. & NI, J. F. 1994. Pn velocities beneath continental collision zones: the Turkish-Iranian Plateau. *Geophysical Journal International*, **117**, 273–283.
- HETÉNYI, G. 2007. *Evolution of deformation of the Himalayan prism: from imaging to modelling*. PhD thesis, Université de Paris Sud XI.
- JIANG, M., GALVÉ, A. *ET AL.* 2006. Crustal thickening and variations in architecture from the Qaidam basin to the Qang Tang (North-Central Tibetan Plateau) from wide-angle reflection seismology. *Tectonophysics*, **412**, 121–140.
- JIMÉNEZ-MUNT, I., FERNÁNDEZ, M., VERGÉS, J. & PLATT, J. P. 2008. Lithosphere structure underneath the Tibetan Plateau inferred from elevation, gravity and geoid anomalies. *Earth and Planetary Science Letters*, **267**, 276–289.
- JIMÉNEZ-MUNT, I., FERNÁNDEZ, M., VERGÉS, J., GARCIA-CASTELLANOS, D., FULLEA, J., PÉREZ-GUSSINYÉ, M. & AFONSO, J. C. 2011. Decoupled accommodation of Africa-Eurasia convergence in the NW-Moroccan margin. *Journal of Geophysical Research*, **116**, B08403, <https://doi.org/10.1029/2010JB008105>
- JIMÉNEZ-MUNT, I., FERNÁNDEZ, M., SAURA, E., VERGÉS, J. & GARCIA-CASTELLANOS, D. 2012. 3D lithospheric structure and regional/residual Bouguer anomalies from Arabia-Eurasia collision in Iran. *Geophysical Journal International*, **190**, 1311–1324.
- KAO, H., GAO, R., RAU, R. J., SHI, D., CHEN, R. Y., GUAN, Y. & WU, F. T. 2001. Seismic image of the Tarim Basin and its collision with Tibet. *Geology*, **29**, 575–578.
- KARUNAKARAN, C. & RAO, A. R. 1979. *Status of Exploration for Hydrocarbons in the Himalayan Region – Contribution to Stratigraphy and Structure*. Geological Survey of India, Miscellaneous Publications, **41**, 1–66.
- KAZMIN, V. G., SBORTSHIKOV, I. M., RICOU, L.-E., ZONENSHAIN, L. P., BOULIN, J. & KNIPPER, A. L. 1986. Volcanic belts as markers of the Mesozoic–Cenozoic active margin of Eurasia. *Tectonophysics*, **123**, 123–152.
- KIND, R., YUAN, X. *ET AL.* 2002. Seismic images of crust and upper mantle beneath Tibet: evidence for Eurasian Plate subduction. *Science*, **298**, 1219–1221.
- KUMAR, M. R., SAUL, J., SARKAR, D., KIND, R. & SHUKLA, A. K. 2001. Crustal structure of the Indian shield: new constraints from teleseismic receiver functions. *Geophysical Research Letters*, **28**, 1339–1342.
- KUMAR, P., YUAN, X., KIND, R. & KOSAREV, G. 2004. Crustal structure variations in northeast India from converted phases. *Geophysical Research Letters*, **31**, L17605.
- KUMAR, P., YUAN, X., KIND, R. & KOSAREV, G. 2005. The lithosphere–asthenosphere boundary in the Tien Shan–Karakoram region from S receiver functions: evidence for continental subduction. *Geophysical Research Letters*, **32**, L07305.
- KUMAR, P., YUAN, X., KUMAR, M. R., KIND, R., LI, X. & CHADHA, R. K. 2007. The rapid drift of the Indian tectonic plate. *Nature*, **449**, 894–897.
- LASKE, G., MASTERS, G., MA, Z. & PASYANOS, M. 2013. Update on CRUST1.0 – a 1-degree global model of earth's crust. *Geophysical Research Abstracts*, **15**, EGU2013–EGU2658.
- LI, A. & MASHELE, B. 2009. Crustal structure in the Pakistan Himalaya from teleseismic receiver functions. *Geochemistry, Geophysics, Geosystems*, **10**, Q12010.
- LI, Q., GAO, R. *ET AL.* 2001. An explosive seismic sounding profile across the transition zone between West Kunlun Mts and Tarim Basin. *Science in China Series D: Earth Sciences*, **44**, 666–672.
- LI, Y., WU, Q., ZHANG, R., TIAN, X. & ZENG, R. 2008. The crust and upper mantle structure beneath Yunnan from joint inversion of receiver functions and Rayleigh wave dispersion data. *Physics of Earth and Planetary Interiors*, **170**, 134–170.
- LIANG, X., SANDVOL, E. *ET AL.* 2012. A complex Tibetan upper mantle: a fragmented Indian slab and no south-verging subduction of Eurasian lithosphere. *Earth and Planetary Science Letters*, **333–334**, 101–111.
- LOU, H., WANG, C. Y., LU, Z. Y., YAO, Z. X., DAI, S. G. & YOU, H. C. 2009. Deep tectonic setting of the 2008

- Wenchuan M_s 8.0 earthquake in southwestern China – joint analysis of teleseismic P-wave receiver functions and Bouguer gravity anomalies. *Science in China Series D: Earth Sciences*, **52**, 166–179.
- MANGINO, S. & PRIESTLEY, K. 1998. The crustal structure of the Southern Caspian region. *Geophysical Journal International*, **133**, 630–648.
- MAHONEY, J. J. 1988. Deccan traps. In: MACDOUGALL, J. D. (ed.) *Continental Flood Basalts*. Kluwer, Dordrecht, 151–194.
- MAKAROV, V. I., ALEKSEEV, D. V. *ET AL.* 2010. Underthrusting of Tarim beneath the Tien Shan and deep structure of their junction zone: main results of seismic experiment along MANAS Profile Kashgar-Song-Kol. *Geotectonics*, **44**, 102–126.
- McKENZIE, D. & BOWIN, C. 1976. The relationship between bathymetry and gravity in the Atlantic Ocean. *Journal of Geophysical Research*, **81**, 1903–1915.
- MCQUARRIE, N. & VAN HINSBERGEN, D. J. J. 2013. Retro-deforming the Arabia-Eurasia collision zone: age of collision v. magnitude of continental subduction. *Geology*, **41**, 315–318.
- MECHIE, J., YUAN, X. *ET AL.* 2012. Crustal and uppermost mantle velocity structure along a profile across the Pamir and southern Tien Shan as derived from project TIPAGE wide-angle seismic data. *Geophysical Journal International*, **188**, 385–407.
- MEISSNER, R., TILMANN, F. & HAINES, S. 2004. About the lithospheric structure of Central Tibet, based on seismic data from the Indepth III profile. *Tectonophysics*, **380**, 1–25.
- MELLORS, R., GÖK, R., PASYANOS, M., SKOBELTSYN, G., TEOMAN, U., GODOLADZE, T. & SANDVOL, E. 2008. High-resolution seismic velocity and attenuation models of the Caucasus–Caspian region. In: *Proceedings of the 30th Monitoring Research Review: Ground-based Nuclear Explosion Monitoring Technologies 23–25 September 2008*, Portsmouth, VA, Volume 1. United States Air Force Research Laboratory, Hanscom AFM, MA, 142–150.
- MI, N., WANG, L. S. *ET AL.* 2005. Velocity structure of the crust and uppermost mantle in the boundary area of the Tianshan Mountains and the Tarim Basin. *Chinese Science Bulletin*, **50**, 270–275.
- MITRA, S., PRIESTLEY, K., BHATTACHARYYA, A. K. & GAUR, V. K. 2005. Crustal structure and earthquake focal depths beneath northeastern India and Southern Tibet. *Geophysical Journal International*, **160**, 227–248.
- MITRA, S., PRIESTLEY, K., GAUR, V. K. & RAI, S. S. 2006. Shear-wave structure of the South Indian lithosphere from Rayleigh wave phase-velocity measurements. *Bulletin of Seismological Society of America*, **96**, 1551–1559.
- MITRA, S., BHATTACHARYA, S. N. & NATH, S. K. 2008. Crustal structure of the western Bengal basin from joint analysis of teleseismic receiver functions and Rayleigh-wave dispersion. *Bulletin of the Seismological Society of America*, **98**, 2715–2723.
- MOHSEN, A., KIND, R. & SOBOLEV, S. M. & THE DESERT GROUP 2006. Thickness of the lithosphere East of the Dead Sea Transform. *Geophysical Journal International*, **167**, 845–852.
- MOKHTAR, T. A., AMMON, C. A., GHALIB, R. B. & HERRMANN, A. A. 2001. Surface wave velocity across Arabia. *Pure and Applied Geophysics*, **158**, 1425–1440.
- MOONEY, W. D., LASKE, G. & MASTERS, T. G. 1998. CRUST 5.1: a global crustal model at 5×5 . *Journal of Geophysical Research*, **103**, 727–747.
- MOTAGHI, K., TATAR, M. & PRIESTLEY, K. 2012. Crustal thickness variation across the northeast Iran continental collision zone from teleseismic converted waves. *Journal of Seismology*, **16**, 253–260.
- MOTAVALLI-ANBARAN, S.-H., ZEYEN, H., BRUNET, M.-F. & ARDESTANI, V. E. 2011. Crustal and lithospheric structure of the Alborz mountains, Iran, and surrounding areas from integrated geophysical modeling. *Tectonics*, **30**, TC5012.
- MOUTHEREAU, F., LACOMBE, O. & VERGÉS, J. 2012. Building the Zagros collisional orogen: timing, strain distribution and the dynamics of Arabia/Eurasia plate convergence. *Tectonophysics*, **532–535**, 27–60.
- NABELEK, J., HETÉNYI, G. *ET AL.* 2009. Underplating in the Himalaya-Tibet collision zone revealed by the Hi-CLIMB experiment. *Science*, **325**, 1371–1374.
- NAQVI, S. M. & ROGERS, J. J. W. 1987. *Precambrian Geology of India*. Oxford Monographs on Geology and Geophysics, **6**. Oxford University Press, New York.
- NASRABADI, A., TATAR, M., PRIESTLEY, K. & SEPAHVAND, M. R. 2008. Continental lithosphere structure beneath the Iranian Plateau, from analysis of receiver functions and surface waves dispersion. Paper presented at the 14th World Conference on Earthquake Engineering, 12–17 October 2008, Beijing, China.
- NATAF, H.-C. & RICARD, Y. 1996. 3SMAC: an a priori tomographic model of the upper mantle based on geophysical modeling. *Physics of the Earth and Planetary Interiors*, **95**, 101–122.
- NOWROUZI, G., PRIESTLEY, K., GHAFORY-ASHTIANY, M., DOLOEI, J. & RHAM, D. 2007. Crustal velocity structure in the Kopet-Dagh from analysis of P-waveform receiver functions. *Journal of Seismology and Earthquake Engineering*, **8**, 187–194.
- ORSHIN, S., KISELEV, S., VINNIK, L., PRAKASAM, K. S., RAI, S. S., MAKEYEVA, L. & SAVVIN, Y. 2008. Crust and mantle beneath western Himalaya, Ladakh and Western Tibet from integrated seismic data. *Earth and Planetary Science Letters*, **271**, 75–87.
- OWENS, T. J. & ZANDT, G. 1997. Implications of crustal property variations for models of Tibetan Plateau evolution. *Nature*, **387**, 37–43.
- PAN, S. & NIU, F. 2011. Large contrasts in crustal structure and composition between the Ordos Plateau and the NE Tibetan Plateau from receiver function analysis. *Earth and Planetary Science Letters*, **303**, 291–298.
- PAUL, A., KAVIANI, A., HATZFELD, D., VERGNE, J. & MOKHTARI, M. 2006. Seismological evidence for crustal-scale thrusting in the Zagros mountain belt (Iran). *Geophysical Journal International*, **166**, 227–237.
- PAUL, A., HATZFELD, D., KAVIANI, A., TATAR, M. & PEQUEGNAT, C. 2010. Seismic imaging of the lithospheric structure of the Zagros mountain belt (Iran).

- In: LETURMY, P. & ROBIN, C. (eds) *Tectonic and Stratigraphic Evolution of Zagros and Makran during the Mesozoic–Cenozoic*. Geological Society, London, Special Publications, **330**, 5–18, <https://doi.org/10.1144/SP330.2>
- PAVLIS, N. K., HOLMES, S. A., KENYON, S. C. & FACTOR, J. K. 2008. An Earth gravitational model to degree 2160. In: *Abstracts of the European Geosciences Union, General Assembly 2008, Vienna. Geophysical Research Abstracts*, **10**, EGM2008.
- PRAJAPATI, S., CHAUHAN, M., GUPTA, A. K., PRADHAN, R., SURESH, G. & BHATTACHARYA, S. N. 2011. Shield-like lithosphere of the lower Indus Basin evaluated from observations of surface-wave dispersion. *Bulletin of Seismological Society of America*, **101**, 859–865.
- PRIESTLEY, K., DEBAYLE, E., MCKENZIE, D. & PILIDOU, S. 2006. Upper mantle structure of eastern Asia from multimode surface waveform tomography. *Journal of Geophysical Research: Solid Earth*, **111**, 2156–2202.
- PRIESTLEY, K., MCKENZIE, D., BARRON, J., TATAR, M. & DEBAYLE, E. 2012. The Zagros core: deformation of the continental lithospheric mantle. *Geochemistry, Geophysics, Geosystems*, **13**, Q11014.
- PUBELLIER, M., CHAMOT-ROOKE, N., EGO, F., GUÉZOU, J. C., KONSTANTINOVSKAYA, E., RABAUTE, A. & RINGENBACH, J. C. 2008. Structural map of Eastern Eurasia. Commission for the Geological Map of the World (CGMW), Paris.
- QIUSHENG, L., RUI, G. ET AL. 2002. Tarim underthrust beneath western Kunlun: evidence from wide-angle seismic sounding. *Journal of Asian Earth Sciences*, **20**, 247–253.
- RADHAKRISHNA, M., TWINKLE, D. ET AL. 2012. Crustal structure and rift architecture across the Krishnaegodavari Basin in the central eastern continental margin of India based on analysis of gravity and seismic data. *Marine and Petroleum Geology*, **37**, 129–146.
- RADJAE, A., RHAM, D., MOKHTARI, M., TATAR, M., PRIESTLEY, K. & HATZFELD, D. 2010. Variation of Moho depth in the central part of the Alborz mountains, Northern Iran. *Geophysical Journal International*, **181**, 173–184.
- RAMESH, D. S., BIANCHI, M. B. & SHARMA, S. D. 2010. Images of possible fossil collision structures beneath the eastern Ghats Belt, India, from P and S receiver functions. *Lithosphere*, **2**, 84–92.
- RAO, M. B. R. 1973. The subsurface geology of the Indo-Gangetic plains. *Journal of Geological Society of India*, **14**, 217–242.
- REGUZZONI, M., SAMPIETRO, D. & SANS, F. 2013. Global Moho from the combination of the CRUST2.0 model and GOCE data. *Geophysical Journal International*, **195**, 222–237.
- REPLUMAZ, A., GUILLOT, S., VILLASEÑOR, A. & NEGREDO, A. M. 2013. Amount of Asian lithospheric mantle subducted during the India/Asia collision. *Gondwana Research*, **24**, 936–945.
- RITSEMA, J., DEUSS, A., VAN HEIJST, H. J. & WOODHOUSE, J. H. 2011. S4ORTS: a degree-40 shear-velocity model for the mantle from new rayleigh wave dispersion, teleseismic traveltimes and normal-mode splitting function measurements. *Geophysical Journal International*, **184**, 1223–1236.
- RITZWOLLER, M. H. & LEVSHIN, A. L. 1998. Eurasian surface wave tomography: group velocities. *Journal of Geophysical Research*, **103**, 4839–4878.
- ROBERT, A., PUBELLIER, M. ET AL. 2010a. Structural and thermal characters of the Longmen Shan (Sichuan, China). *Tectonophysics*, **491**, 165–173.
- ROBERT, A., ZHU, J. ET AL. 2010b. Crustal structures in the area of the 2008 Sichuan earthquake from seismologic and gravimetric data. *Tectonophysics*, **491**, 205–210.
- ROBERT, A., LETOUZEY, J., MÜLLER, C., KAVOOSI, M., VERGÉS, J., SHERKATI, S. & AGHABABEI, A. 2014. Structural evolution of the Kopeh Dagh fold-and-thrust belt (NE Iran) and interactions with the South Caspian and Amu Darya basins. *Journal of Marine and Petroleum Geology*, **57**, 68–87.
- ROSS, A. R., BROWN, L. D. ET AL. 2004. Deep reflection surveying in Central Tibet: lower-crustal layering and crustal flow. *Geophysical Journal International*, **156**, 115–128.
- ROWLEY, D. B. 1996. Age of initiation of collision between India and Asia: a review of stratigraphic data. *Earth and Planetary Science Letters*, **145**, 1–13.
- SANDVOL, E., SEBER, D., CALVERT, A. & BARAZANGI, M. 1998. Grid search modeling of receiver functions: implications for crustal structure in the Middle East and North Africa. *Journal of Geophysical Research*, **103**, 26,899–26,917.
- SASTRI, V. V., BHANDARI, L. L., RAJU, A. T. R. & DUTTA, A. K. 1971. Tectonic framework and subsurface stratigraphy of the Ganga Basin. *Journal of Geological Society of India*, **12**, 222–233.
- SCHULTE-PEKLUM, V., MONSALVE, G., SHEEHAN, A., PANDEY, M. R., SAPKOTA, S., BILHAM, R. & WU, F. 2005. Imaging the Indian subcontinent beneath the Himalaya. *Nature*, **435**, 1222–1225.
- SENGÖR, A. M. C. & NATAL'IN, B. A. 1996. Palaeotectonics of Asia: fragments of a synthesis. In: YIN, A. & HARRISON, M. (eds) *Tectonic Evolution of Asia, Rubey Colloquium*. Cambridge University Press, Cambridge, 486–640.
- SENGÖR, A. M. C., ALTINER, D., CIN, A., USTAOMER, T. & HSU, K. J. 1988. Origin and assembly of the Tethyside orogenic collage at the expense of Gondwanaland (in Gondwana and Tethys). In: AUDLEY-CHARLES, M. G. & HALLAM, A. (eds) *Gondwana and Tethys*. Geological Society, London, Special Publications, **37**, 119–181.
- SHI, D., ZHAO, W. ET AL. 2004. Detection of southward intracontinental subduction of Tibetan lithosphere along Bangong-Nujiang suture by P-to-S converted waves. *Geology*, **32**, 209–212.
- SHI, D., SHEN, Y., ZHAO, W. & LI, A. 2009. Seismic evidence for a Moho offset and south-directed thrust at the easternmost Qaidam-Kunlun boundary in the Northeast Tibetan Plateau. *Earth and Planetary Science Letters*, **288**, 329–334.
- SHOMALI, Z. H., KESHVARI, F., HASSANZADEH, J. & MIRZAEI, N. 2011. Lithospheric structure beneath the Zagros collision zone resolved by non-linear teleseismic tomography. *Geophysical Journal International*, **187**, 394–406.

- SINGH, D. D. 1999. Surface wave tomography studies beneath the Indian subcontinent. *Journal of Geodynamics*, **28**, 291–301.
- SINGH, I. B. 1996. Geological evolution of Ganga Plain – an overview. *Journal of the Palaeontological Society of India*, **41**, 99–137.
- SODOUDI, F., YUAN, X., KIND, R., HEIT, B. & SADID-KHOUEY, A. 2009. Evidence for a missing crustal root and a thin lithosphere beneath the central Alborz by receiver function studies. *Geophysical Journal International*, **177**, 733–742.
- SOOMRO, R. A. 2009. *Receiver function analysis for crustal structure beneath Pakistan*. MPhil thesis, Micro Seismic Studies Programme, Islamabad, Pakistan.
- SURESH, G., JAIN, S. & BHATTACHARYA, S. N. 2008. Lithosphere of Indus block in the northwest Indian subcontinent through genetic algorithm inversion of surface-wave dispersion. *Bulletin of the Seismological Society of America*, **98**, 1750–1755.
- TEZEL, T., SHIBUTANI, T. & KAYPAK, B. 2013. Crustal thickness of Turkey determined by receiver function. *Journal of Asian Earth Sciences*, **75**, 36–45.
- TIAN, X., WU, Q., ZHANG, Z., TENG, J. & ZENG, R.-S. 2005. Joint imaging by teleseismic converted and multiple waves and its application in the Indepth-III passive seismic array. *Geophysical Research Letters*, **32**, L21315.
- TIBERI, C., LEROY, S., D'ACREMONT, E., BELLAHSEN, N., EBINGER, C., AL-LAZKI, A. & POINTU, A. 2007. Crustal geometry of the northeastern Gulf of Aden passive margin: localization of the deformation inferred from receiver function analysis. *Geophysical Journal International*, **168**, 1247–1260.
- TILMANN, F. 2011. *Seismic Investigation of the Northern Tibetan Margin*. Loan 769: Final Report
- TONG, W., WANG, L. ET AL. 2007. Receiver function analysis for seismic structure of the crust and uppermost mantle in the Liupanshan area, China. *Science in China Series D: Earth sciences*, **50**, 227–233.
- VERGÉS, J., SAURA, E., CASCIELLO, E., FERNÁNDEZ, M., VILLASEÑOR, A., JIMÉNEZ-MUNT, I. & GARCIA-CASTELLANOS, D. 2011. Crustal-scale cross-sections across the NW Zagros Belt: implications for the Arabian margin reconstruction. *Geological Magazine*, **148**, 739–761.
- VERGNE, J., WITTLINGER, G. ET AL. 2002. Seismic evidence for stepwise thickening of the crust across the NE Tibetan Plateau. *Earth and Planetary Science Letters*, **203**, 25–33.
- VILÀ, M., FERNÁNDEZ, M. & JIMÉNEZ-MUNT, I. 2010. Radiogenic heat production variability of some common lithological groups and its significance to lithospheric thermal modeling. *Tectonophysics*, **490**, 152–164.
- VILLASEÑOR, A., RITZWOLLER, M. H., LEVSHIN, A. L., BARMIN, M. P., ENGDahl, E. R., SPAKMAN, W. & TRAMPERT, J. 2001. Shear velocity structure of Central Eurasia from inversion of surface wave velocities. *Physics of the Earth and Planetary Interiors*, **123**, 169–184.
- VINNIK, L. P., REIGBER, C., ALESHIN, I. M., KOSAREV, G. L., KABAN, M. K., ORESHIN, S. I. & ROECKER, S. W. 2004. Receiver function tomography of the Central Tien Shan. *Earth and Planetary Science Letters*, **225**, 131–146.
- WANG, C.-Y., WU, J. P., LOU, H., ZHOU, M. & BAI, Z. 2003. P-wave crustal velocity structure in western Sichuan and eastern Tibetan region. *Science in China Series D: Earth Sciences*, **46**, 254–265.
- WANG, C.-Y., YANG, Z.-E., LUO, H. & MOONEY, W. D. 2004. Crustal structure of the northern margin of the Eastern Tien Shan, China, and its tectonic implications for the 1906 M 7.7 Manas earthquake. *Earth and Planetary Science Letters*, **223**, 181–202.
- WANG, C. Y., LOU, H., SILVER, P. G., ZHU, L. & CHA, L. 2010. Crustal structure variation along 30°N in the Eastern Tibetan Plateau and its tectonic implications. *Earth and Planetary Science Letters*, **289**, 367–376.
- WESSEL, P. & SMITH, W. H. F. 1991. Free software helps map and display data. *Eos, Transactions of the American Geophysical Union*, **72**, 441–446.
- WILHEM, C., WINDLEY, B. F. & STAMPFLI, G. M. 2012. The Altaids of Central Asia: a tectonic and evolutionary innovative review. *Earth-Science Reviews*, **113**, 303–341.
- WITTLINGER, G., VERGNE, J. ET AL. 2004. Teleseismic imaging of subducting lithosphere and Moho offsets beneath Western Tibet. *Earth and Planetary Science Letters*, **221**, 117–130.
- XU, Q., ZHAO, J., PEI, S. & LIU, H. 2013. Distinct lateral contrast of the crustal and upper mantle structure beneath northeast Tibetan Plateau from receiver function analysis. *Physics of the Earth and Planetary Interiors*, **217**, 1–9.
- YAMINIFARD, F., SEDGHI, M. H., GHOLAMZADEH, A., TATAR, M. & HESSAMI, K. 2012. Active faulting of the southeastern-most Zagros (Iran): microearthquake seismicity and crustal structure. *Journal of Geodynamics*, **55**, 56–65.
- YIN, A. & HARRISON, M. 2000. Geologic evolution of the Himalayan Tibetan Orogen. *Annual Review of Earth and Planetary Sciences*, **28**, 211–280.
- YUE, H., CHEN, Y. J. ET AL. 2012. Lithospheric and upper mantle structure of the northeastern Tibetan Plateau. *Journal of Geophysical Research: Solid Earth*, **117**, 2156–2202.
- ZHANG, X. & WANG, Y. 2009. Crustal and upper mantle velocity structure in Yunnan, Southwest China. *Tectonophysics*, **471**, 171–185.
- ZHAO, J., LIU, G., LU, Z., ZHANG, X. & ZHAO, G. 2003. Lithospheric structure and dynamic processes of the Tianshan orogenic belt and the Junggar Basin. *Tectonophysics*, **376**, 199–239.
- ZHAO, J., MOONEY, W. D., ZHANG, X., LI, Z., JIN, Z. & OKAYA, N. 2006. Crustal structure across the Altyn Tagh range at the northern margin of the Tibetan Plateau and tectonic implications. *Earth and Planetary Science Letters*, **241**, 804–814.
- ZHAO, J., YUAN, X. ET AL. 2010. The boundary between the Indian and Asian tectonic plates below Tibet. *Proceedings of the National Academy of Sciences*, **107**, 11229–11233.
- ZHAO, W., MECHIE, J. ET AL. 2001. Crustal structure of Central Tibet as derived from project Indepth wide-angle seismic data. *Geophysical Journal International*, **145**, 486–498.

- ZHAO, W., KUMAR, P. *ET AL.* 2011. Tibetan Plate overriding the Asian Plate in Central and Northern Tibet. *Nature Geoscience*, **4**, 870–873.
- ZHU, B., KIDD, W., ROWLEY, D. B., CURRIE, B. & SHAFIQUE, N. 2005. Age of initiation of the India-Asia collision in the East-Central Himalaya. *Journal of Geology*, **113**, 265–285.
- ZOR, E., SANDVOL, E., GÜRBÜZ, C., TÜRKELLI, N., SEBER, D. & BARAZANGI, M. 2003. The crustal structure of East Anatolian Plateau (Turkey) from receiver functions. *Geophysical Research Letters*, **30**, 8044.
- ZORIN, Y., MORDVINOVA, V., TURUTANOV, E., BELICHENKO, B., ARTEMYEV, A., KOSAREV, G. & GAO, S. 2002. Low seismic velocity layers in the Earth's crust beneath Eastern Siberia (Russia) and Central Mongolia: receiver function data and their possible geological implication. *Tectonophysics*, **359**, 307–327.